

# Improving Stability and Adaptability of Automotive Electric Steering Systems Based on a Novel Optimal Integrated Algorithm

## Abstract:

This research proposes a new algorithm to control the Electric Power Steering (EPS) systems of automobiles. The algorithm combines Proportional Integral Derivative (PID) control and Sliding Mode Control (SMC) with parameters optimized by a Genetic Algorithm (GA). These optimal parameters are dynamically adjusted by a fuzzy algorithm having three inputs. The proposed algorithm is named as Fuzzy Proportional Integral Derivative Sliding Mode Control–Genetic Algorithm (FPIDSMC–GA). The algorithm helps to improve the system stability and is capable of adapting as per requirements of several complex conditions. The effectiveness of the new algorithm has been evaluated by numerical simulations conducted in MATLAB/Simulink environment. The value of the road disturbance is varied to investigate the system's stability. Simulation results confirm that the values of the motor angle and steering column angle closely track the reference signal under different conditions when the proposed FPIDSMC-GA based control algorithm is applied to control the EPS system. The tracking error increases as the road reaction torque increases. The control effort varies with the changes in the road reaction torque and reference signal, however, it is still within the allowable limit. The system adaptation and stability are guaranteed in the investigated cases. The average errors in motor angle and steering angle are found to be  $0.63^\circ$  and  $0.07^\circ$  respectively with the maximum errors not exceeding  $5.73^\circ$  and  $0.81^\circ$ .

**Keywords:** Electric steering system; FPIDSMC-GA; intelligent optimal integrated control; motor angle.

## Abbreviation

ACO	Ant colony optimization	LPV	Linear parameter varying
ADRC	Active disturbance rejection control	LQG	Linear Gaussian regulator
ANN	Artificial neural network	LQR	Linear quadratic regulator
BCGA	Binary code genetic algorithm	MIMO	Multi input Multi output
BPNN	Back propagation neural network	MPC	Model predictive control
EHPS	Electro-hydraulic power steering	PID	Proportional Integral Derivative
EPS	Electric power steering	RMS	Root mean square
GA	Genetic algorithm	SISO	Single input - Single output
HPS	Hydraulic power steering	SMC	Sliding mode control

## 1. Introduction

### 1.1. The EPS system and literature review

Most cars today use a power steering system, which are divided into three basic categories: hydraulic, electro-hydraulic, and electric power steering. Hydraulic steering systems are usually used in older cars or large trucks. However, a Hydraulic Power Steering (HPS) system still has

many disadvantages that cannot be resolved. According to Baek and Kang [1], the HPS system reduces the engine's efficiency and negatively impacts the environment because it uses a hydraulic system. Additionally, this system is quite bulky because it has many devices, such as oil pumps, reservoirs, etc. Electric Power Steering (EPS) systems have many advantages compared to traditional hydraulic steering systems. According to Li *et al.* [2], electric driving systems are safe, energy-efficient, and environmentally friendly. In addition, the EPS system has higher sensitivity and a smaller size compared to the HPS system. According to Choi *et al.* [3], the EPS system helps to improve the feelings while steering feel when the vehicle moves in many different conditions. These are outstanding advantages that only belong to the EPS system.

EPS are commonly used on high-end sedans, SUVs [4], or other terrain vehicles [5]. The general structure of an EPS usually includes a steering wheel and column, an electric motor, a gearbox, and several sensors. The electric motor can be mounted on a column, rack, or pinion [6]. Some older vehicle models use recirculating ball and worm gear instead of rack and pinion [7]. There are many factors that affect the performance of the EPS system. In [8], Kim *et al.* indicated that crosswind disturbances can negatively affect the EPS system. This is also confirmed by Jung and Kim in [9]. In addition, road reaction torque also has a significant influence on steering [10]. The value of road reaction torque can be estimated based on a new method proposed by Jang *et al.* [11]. In modern or self-driving vehicles, the EPS system is often combined with the steer-by-wire system to form a complex modern steering system.

Many studies relating to EPS system control have been reported recently. These control algorithms can be divided into two main categories: linear control and nonlinear control [12]. These two categories can be combined with some intelligent control algorithms. The PID algorithm is commonly used in EPS systems today. This is a simple algorithm that serves the control objectives, but it can be highly effective if we can choose the controller parameters optimally. In [13], Hassan *et al.* designed an optimal PID algorithm to control cars' EPS system. They used Binary-Coded Genetic Algorithm (BCGA) to find the optimal parameters  $k_P$ ,  $k_I$ , and  $k_D$  for the controller. The objective function of the optimal process is determined by mean-squared error, according to Hassan *et al.* genetic algorithms are also commonly used in automobiles, mechatronics, and other general fields [14]. The electric motor's current is quite large, up to 50 A. Using large currents can cause several potential dangers and increase energy consumption. Therefore, Hanifah *et al.* propose using Ant Colony Optimization (ACO) algorithm to find suitable values for the PID controller to reduce energy consumption [15]. This algorithm is further improved in [16] by Hanifah *et al.* As a result, its convergence is further enhanced. The results demonstrate that the current average value approaches the Root Mean Square (RMS) value when the PID-ACO algorithm is used instead of the conventional PID. In addition, we can use fuzzy algorithms to dynamically tune the controller parameters to respond to specific conditions instead of just finding an optimal value. This is highlighted by Zheng and Wei [17]. In [18], Hassan *et al.* claimed that a fuzzy-PID controller can help to reduce the energy consumption of EPS systems better than traditional PID. In addition, other algorithms, such as Back Propagation Neural Network (BPNN) or in-loop, are also used to find suitable values for the PID controller [19, 20]. PID algorithm is mainly suitable for Single Input Single Output (SISO) systems. If the system has Multiple Inputs Multiple Outputs (MIMO), Linear Quadratic Regulator (LQR) and other algorithms can be used.

In [21], Chitu *et al.* designed an LQR solution to control the EPS system. The main goal of this technique is to minimize the cost function of the system. External interference signals can affect the quality of the LQR controller. Therefore, Irmer and Henrichfreise additionally designed a Gaussian compensator for the system, so it became LQG [22]. Another linear control technique Linear Parameter-Varying (LPV) has also been applied to the EPS system [23].

The controlled object is usually motor angle [24, 25] or assisted torque [26]. The road disturbance is nonlinear; therefore, we should use nonlinear control algorithms for the EPS system instead of conventional linear control [19]. In [27], Lee *et al.* presented simulation results from different linear and nonlinear controllers for an EPS system. These results show that the nonlinear control algorithm performs more efficiently under different conditions. According to Ma *et al.* [28], these algorithms can eliminate disturbance from the road surface. Lee *et al.* proposed a robust control algorithm for the EPS system by tracking steering wheel torque [29]. A 3D map depicting the relationship among steering wheel torque, steering wheel velocity, and steering wheel angle is given in [29]. Besides, simulation results show that measured and estimated steering wheel angle values are always close together while steering wheel velocity and acceleration are chattered. Many researchers have applied  $H_\infty$  control algorithm to EPS systems, such as Dannöhl *et al.* [30], Zhao *et al.* [31], etc. The results in [31] show that the response of the  $H_\infty$  controller is more efficient than conventional PID, while PID is more responsive than  $H_2$ , according to Zhang *et al.* [31]. A combination of  $H_2$  and  $H_\infty$  is performed by Zhao *et al.* [32] demonstrating that the value of steering wheel torque is significantly reduced when both algorithms  $H_2$  and  $H_\infty$  are applied.

SMC algorithm can help to ensure system stability in the presence of external nonlinear disturbances. This algorithm can be applied to many mechatronic or automotive control systems [33-36]. Designing a sustainable SMC algorithm is not trivial because this process involves the higher-order derivative [36]. Recently, Kim *et al.* [37] proposed a steering wheel torque control method based on the SMC principle. The results show that system performance can be improved while maintaining stability against external disturbances. The reliability of this algorithm is verified by experiments in the discrete-time domain as reported in [38]. SMC algorithm can be combined with several other algorithms to improve the control performance, such as fuzzy-SMC [39, 40], backstepping-SMC [41], and fuzzy ANN-SMC [42]. Some other nonlinear control algorithms, such as MPC [43, 44], ADRC [45], or nonlinear hybrid [46] have also applied to EPS systems. Optimization algorithms such as non-dominated sorting GA [47], multi-objective GA [48], and optimal GA [49] can help optimize controller parameters. In contrast, the Takagi-Sugeno fuzzy algorithm can flexibly adjust these values [50].

## ***1.2.Motivation and contribution***

Most of the aforementioned algorithms are usually used in a single form or as a combination of two-component algorithms. They can guarantee efficiency under certain conditions that are suitable for component algorithms. However, they still have some unresolved drawbacks summarized below:

- 1) Some algorithms like PID, LQR, LQG, etc. are highly effective only in linear oscillatory conditions. The controller's performance can be significantly degraded when the system is subjected to external nonlinear influences, such as disturbances or uncertainties [22, 23, 27].
- 2) The chattering phenomenon still occurs when applying only a single linear or a nonlinear algorithm, such as LPV [23], lead-lag control [27], ADRC [24], SMC [29, 33], MPC [45] etc., in contrast to applying integrated nonlinear algorithms. This can negatively affect the quality of the EPS system.
- 3) For controllers whose parameters are optimized using optimal search algorithms such as GA [13, 14], ACO [15], PSO [16], or in-loop model [20], the system response only reaches the optimal state under one or a few specific conditions. These conditions must satisfy the optimal requirements of the algorithm. When the system is affected by other conditions, the optimal state will not be guaranteed.
- 4) Using intelligent algorithms, such as fuzzy [17, 18] or BPNN [19], to flexibly adjust the controller's parameters is a highly effective solution. This helps the system adapt well to external influences. However, the algorithm's structure (such as membership functions, fuzzy rules, etc.) is primarily driven by the control designer's experience. Therefore, the adjustment range of the algorithm can be optimal or suboptimal.

In order to solve these problems, we propose designing a novel intelligent optimization algorithm to control the EPS system. The novelty of the proposed work lies in integrating the SMC technique and PID algorithm and getting inspiration from fuzzy logic and GA. The PID controller parameters are optimally selected through GA. These parameters are then dynamically fine-tuned by a fuzzy algorithm that takes three inputs. In this way, the intelligent optimal controller can adapt to several external conditions. Additionally, this combination helps to eliminate the chattering phenomenon that exists when using a standalone control algorithm such as SMC. To the best of authors' knowledge, this is an entirely new method that does not seem to have been applied as of now to control automotive EPS system. This idea is a remarkable extension to our earlier work reported in [51]. However, the structure of the control system in the present study is significantly different from the one given in [51]. In addition, in the present study, the controller parameters are optimally calculated before undergoing tuning using a fuzzy algorithm. This is considered as new contribution to solve existing problems in automotive EPS systems.

The remaining article is organized as follows: Section 1 introduces the EPS system and reviews the state of the arts. Section 2 presents the mathematical model of the system. Section 3 reports simulation results obtained after applying the proposed control strategy to the derived model. Finally, Section 4 comments on the conclusion.

## **2. Material**

The model of an EPS system is shown in Figure 1. The system is divided into two main parts: the mechanical part (steering wheel, steering column, and steering gearbox) and the electrical part (electric motor, ECU, and sensors). The operation of a steering system is described in (1-3).

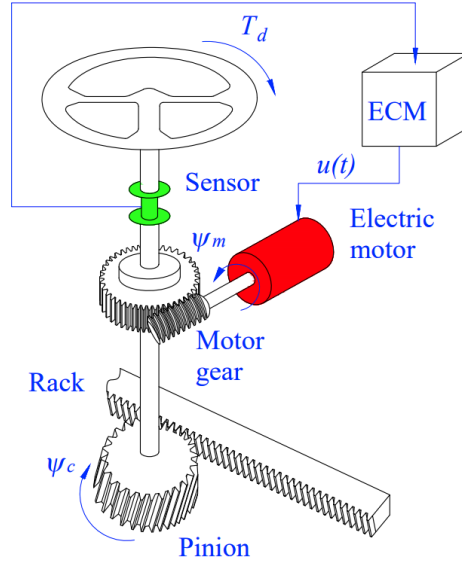


Figure 1. Electric power steering system

$$I_c \ddot{\psi}_c + B_c \dot{\psi}_c + K_c \psi_c = \frac{K_c}{N} \psi_m + T_d \quad (1)$$

$$\left( I_m + \frac{r_p^2}{N^2} M_r \right) \ddot{\psi}_m + \left( B_m + \frac{r_p^2}{N^2} B_r \right) \dot{\psi}_m + \frac{K_c + K_r r_p^2}{N^2} \psi_m = \frac{K_c}{N} \psi_c + T_d + K_t i_m(t) - \frac{T_r}{N} \quad (2)$$

$$L_m \dot{i}_m(t) + R_m i_m(t) = u(t) - K_t \dot{\psi}_m \quad (3)$$

The nomenclature used in (1-3) is presented in Table 1.

Table 1. Symbol and description

Symbol	Description	Unit	Symbol	Description	Unit
$I_c$	Moment of inertia (steering column)	$\text{kgm}^2$	$K_t$	Voltage coefficient (electric motor)	$\text{NmA}^{-1}$
$I_m$	Moment of inertia (electric motor)	$\text{kgm}^2$	$T_d$	Driver torque	Nm
$i_m(t)$	Current (electric motor)	A	$N$	Motor gear ratio	-
$u(t)$	Control signal	v	$\psi_c$	Steering column angle	rad
$B_c$	Damping coefficient (steering column)	$\text{Nmsrad}^{-1}$	$\psi_m$	Electric motor angle	rad
$B_m$	Damping coefficient (electric motor)	$\text{Nmsrad}^{-1}$	$R_m$	Electric motor resistance	$\Omega$

$B_r$	Damping coefficient (rack)	$\text{Nsm}^{-1}$	$r_p$	Pinion radius	m
$K_c$	Torsional stiffness (steering column)	$\text{Nmrad}^{-1}$	$M_r$	Mass or rack	kg
$K_r$	Tire spring rate	$\text{Nm}^{-1}\text{rad}^{-1}$	$L_m$	Electric motor inductance	H

In this study, the control variable is motor angle  $\psi_m$ . Let  $e(t)$  be the error between the desired and output signals i.e.

$$e(t) = -y(t) + y_{ref}(t) \quad (4)$$

The first control signal of the integrated controller is determined by (5), which gives PID control law.

$$u_1(t) = k_p e(t) + k_i \int e(\tau) d\tau + k_d \dot{e}(t) \quad (5)$$

The second control signal indicates the SMC law. Setting the state variables as,

$$x_1 = \psi_c \quad (6)$$

$$x_2 = \dot{\psi}_c = \dot{x}_1 \quad (7)$$

$$x_3 = \psi_m \quad (8)$$

$$x_4 = \dot{\psi}_m = \dot{x}_3 \quad (9)$$

$$x_5 = i_m(t) \quad (10)$$

Taking the derivative of state variables from (6) to (10), we get:

$$\dot{x}_1 = x_2 \quad (11)$$

$$\dot{x}_2 = \sum_{i=1}^5 a_i x_i \quad (12)$$

$$\dot{x}_3 = x_4 \quad (13)$$

$$\dot{x}_4 = \sum_{i=1}^5 b_i x_i \quad (14)$$

$$\dot{x}_5 = \sum_{i=1}^5 c_i x_i + c_6 u(t) \quad (15)$$

where:

$$a_1 = -\frac{K_c}{I_c}$$

$$a_2 = -\frac{B_c}{I_c}$$

$$a_3 = \frac{K_c}{I_c N}$$

$$a_4 = a_5 = 0$$

$$b_1 = \frac{K_c N}{I_m N^2 + r_p^2 M_r}$$

$$b_2 = 0$$

$$b_3 = -\frac{K_c + K_r r_p^2}{I_m N^2 + r_p^2 M_r}$$

$$b_4 = -\frac{B_m N^2 + r_p^2 B_r}{I_m N^2 + r_p^2 M_r}$$

$$b_5 = \frac{K_t N^2}{I_m N^2 + r_p^2 M_r}$$

$$c_1 = c_2 = c_3 = 0$$

$$c_4 = -\frac{K_t}{L_m}$$

$$c_5 = -\frac{R_m}{L_m}$$

$$c_6 = -\frac{1}{L_m}$$

As mentioned above, the signal to be controlled is the motor angle. Therefore,

$$y(t) = x_3 \quad (16)$$

Taking the derivative of (16) five times, we get,

$$\dot{y}(t) = x_4 \quad (17)$$

$$\ddot{y}(t) = \sum_{i=1}^5 b_i x_i \quad (18)$$

$$y^{(3)} = \sum_{i=1}^5 d_i x_i + d_6 u(t) \quad (19)$$

$$y^{(4)} = \sum_{i=1}^5 e_i x_i + e_6 u(t) \quad (20)$$

$$y^{(5)} = \sum_{i=1}^5 f_i x_i + f_6 u(t) \quad (21)$$

where:

$$\begin{aligned} d_1 &= a_1 b_2 + b_1 b_4 + b_5 c_1 & d_2 &= a_2 b_2 + b_1 + b_2 b_4 + b_5 c_2 \\ d_3 &= a_3 b_2 + b_3 b_4 + b_5 c_3 & d_4 &= a_4 b_2 + b_3 + b_4 b_4 + b_5 c_4 \\ d_5 &= a_5 b_2 + b_4 b_5 + b_5 c_5 & d_6 &= b_5 c_6 \\ e_1 &= a_1 d_2 + b_1 d_4 + c_1 d_5 & e_2 &= d_1 + a_2 d_2 + b_2 d_4 + c_2 d_5 \\ e_3 &= a_3 d_2 + b_3 d_4 + c_3 d_5 & e_4 &= a_4 d_2 + d_3 + b_4 d_4 + c_4 d_5 \\ e_5 &= a_5 d_2 + b_5 d_4 + c_5 d_5 & e_6 &= c_6 d_5 \\ f_1 &= a_1 e_2 + b_1 e_4 + c_1 e_5 & f_2 &= a_2 e_2 + b_2 e_4 + c_2 e_5 + e_1 \\ f_3 &= a_3 e_2 + b_3 e_4 + c_3 e_5 & f_4 &= a_4 e_2 + b_4 e_4 + c_4 e_5 + e_3 \\ f_5 &= a_5 e_2 + b_5 e_4 + c_5 e_5 & f_6 &= c_6 e_5 \end{aligned}$$

The derivative component of the control signal is ignored. The sliding surface of the control system  $\gamma(t)$  is given in (22).

$$\gamma(t) = \sum_{i=0}^4 k_i e^{(4-i)t} \quad (22)$$

where  $k_i$  are the coefficients of the polynomial (23) satisfying Hurwitz criterion and  $k_0 = 1$ . A polynomial  $\lambda(s)$  of a complex variable is considered to be the Hurwitz polynomial if the following two conditions are satisfied: 1)  $\lambda(s)$  is real when  $s$  is real; 2) The roots of  $\lambda(s)$  have real parts which are zero or negative.

$$\lambda(s) = \sum_{i=0}^4 k_i s^{4-i} \quad (23)$$

The second control signal obtained from the SMC algorithm can be rewritten as,

$$u_2(t) = \frac{1}{f_6} \left[ y_{ref}^{(5)}(t) - \sum_{i=1}^5 f_i x_i + \sum_{i=1}^4 k_i e^{(5-i)} + K sgn \left( \sum_{i=0}^4 k_i e^{(4-i)} \right) \right] \quad (24)$$

In this work, the stability of the SMC framework is evaluated according to the Lyapunov criterion. A nonlinear Lyapunov control function is chosen as (25). This function is positive definite  $\forall x \neq 0$ .

$$V(x) = \frac{1}{2} \gamma^2 \quad (25)$$

Taking the derivative of (25), we get (26).

$$\dot{V}(x) = \gamma \dot{\gamma} \quad (26)$$

Taking the derivative of the sliding surface (22), we get (27).

$$\dot{\gamma}(t) = \sum_{i=0}^4 k_i e^{(5-i)} \quad (27)$$

Equation (28) is obtained by taking the 5<sup>th</sup> derivative of (4).

$$e^{(5)}(t) = -y^{(5)}(t) + y_{ref}^{(5)}(t) \quad (28)$$

Assuming that the coefficient  $k_0 = 1$ , combining (16), (21), (27), and (28), we get (29).

$$\dot{\gamma} = - \left( \sum_{i=1}^5 f_i x_i + f_6 u(t) \right) + y_{ref}^{(5)}(t) + \sum_{i=1}^4 k_i e^{(5-i)} \quad (29)$$

Substituting (22), (24) and (29) into (26), we get (30). This equation shows that the derivative of the Lyapunov control function is negative definite  $\forall x \neq 0$ . Combining (25) and (30), the system is considered stable.

$$\dot{V}(x) = -\gamma sgn(\gamma) \quad (30)$$

The final control signal is synthesized from the two component signals (Figure 2).

$$u(t) = u_1(t) + u_2(t) \quad (31)$$

This combination provides stability for the system. This has been mentioned in [53, 54]. System performance is guaranteed based on the optimization of controller parameters. These parameters are chosen so that the system's tracking error is minimal.

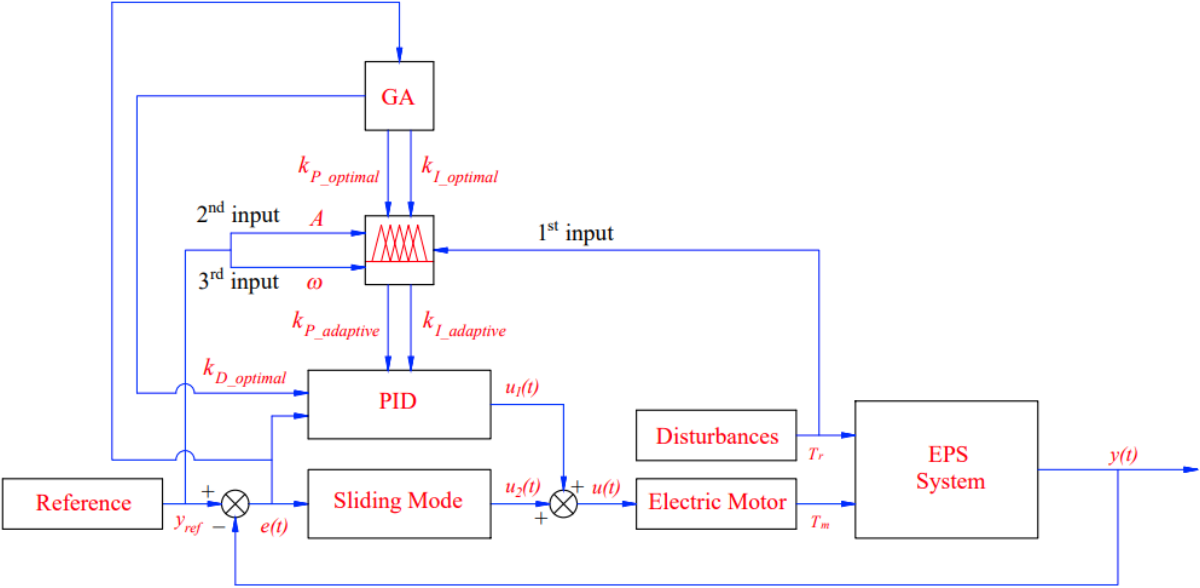


Figure 2. Proposed hybrid control scheme

The coefficients of (5) are optimally selected using a Genetic Algorithm (GA) to ensure that the combination between the two signals is optimal. The proposed algorithm can help determine optimal values under certain conditions and is described through three basic processes: natural selection, crossover, and mutation. The algorithm is conceptualized in Figure 3a.

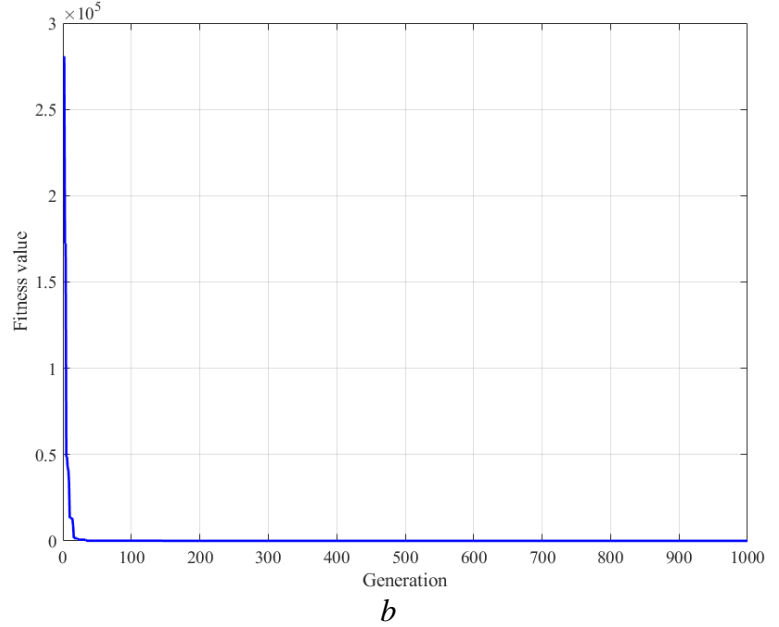
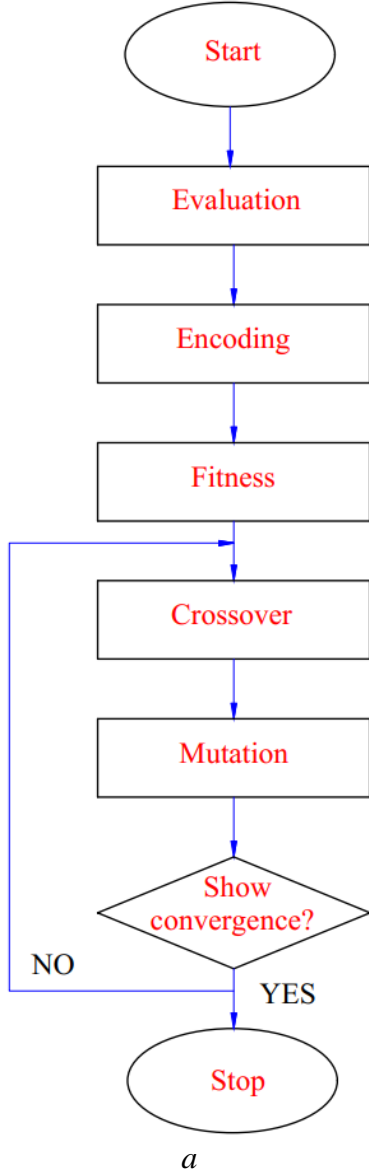


Figure 3. Genetic algorithm

(a) Flow chart of GA (b) Fitness value as a function of generation

Firstly, we need to encode the problem solution by turning it into a sequence of chromosomes. This can be simplified by finding the fitness function  $J(\varphi)$ , where  $\varphi$  is a vector i.e.,

$$\varphi = [\varphi_1, \varphi_2, \varphi_3, \dots, \varphi_n]^T \quad (32)$$

Any sequence of chromosomes is represented as a vector  $\varphi_i$  as follows,

$$\varphi_i = \varphi_{i\_min} + \frac{\varphi_{i\_max} - \varphi_{i\_min}}{2^{L_i} - 1} \sum_{j=0}^{L_i-1} 2^j s_{ij} \quad (33)$$

The length of the binary string  $L_i$  is determined based on the desired precision  $\beta_i$ . We can calculate  $L_i$  through  $\beta_i$  and  $\varphi_i$  as given in (34).

$$L_i = \log_2 \left( \frac{\varphi_{i\_max} - \varphi_{i\_min}}{\beta_i} \right) \quad (34)$$

In the next step, we need to determine the fitness function  $J(\varphi)$  that corresponds to fitness of individuals. So,

$$fitness = J(\varphi) + C \quad (35)$$

where  $C$  is a positive constant. The dominant individuals will then have to go through the process of natural selection. The higher the fitness of chromosomes, the greater their probability of being selected. The intensity of selection ( $I$ ) is determined by (36).

$$I = \frac{M_2 - M_1}{\sigma} \quad (36)$$

where  $M_2$  is the population's average fitness after selection, and  $M_1$  is the population's average fitness before selection.

The subjects then need to go through the crossover process in which chromosomes share information. The offspring chromosomes produced by the parents are expected to be of higher quality. Many studies report that the probability of crossover is quite large. If we use regular crossover, its probability can be as high as 100%, while this number is lower if we use single-point crossover (37) or two-point crossover (38). In general, their values are usually greater than 0.7.

$$p_{c1} = \frac{L-1}{2^{L-1}} \quad (37)$$

$$p_{c2} = \frac{L-1}{2^L} \quad (38)$$

Finally, the offspring chromosomes need to undergo the mutation process. This operation helps to change the genetic structure of individuals to increase diversity in population structure. However, the probability of mutation occurrence is relatively low to avoid disturbing the population.

Each population should be selected based on a specific size. The computation process can converge very quickly if the population size is small, leading to inaccuracy and vice versa. The population size can be determined by (39). In general, if the nonlinearity of the problem increases, the population size also gets increased.

$$N \approx O\left(2^k \frac{\sigma}{d}\right) \quad (39)$$

where  $\sigma^2$  is the variance and  $d^2$  is the difference between the local and global values.

The conditions for the GA computation must be selected appropriately before starting to run the algorithm. The choice of these values can affect the sensitivity of the algorithm.

Firstly, the population size ( $N$ ) should not be chosen too large because it will make the search process more time consuming. On the contrary, if this size is too small, the search scope will be narrow resulting in quick convergence, which leads to an increase in the error value. The population size depends on the length of the chromosome string ( $L$ ) or the deviation of the values according to (39). The population size is optimal when the value of  $L$  is between 20 and 30.

Secondly, the search range is used as a reference solution. The optimal values are determined within this range. The choice of these values depends on the control designer's experience. The present work determines the range of search values based on previous experimental simulation results.

Thirdly, the position of the decimal point and the number of significant digits in encoding significantly affect the optimal values. The accuracy of the results increases as the optimal values increase. However, this may affect the computation speed. Typically, the position of the decimal point is between 2 and 4, while the number of significant digits is between 3 and 6.

Fourthly, the crossover probability is calculated using (37) or (38). As mentioned above, this value is usually between 70% and 100%. If the crossover probability is more significant (approximately 100%), chromosome information from parent to child will not be preserved. In contrast, single-point or two-point crossover methods with a probability of 80% can help preserve chromosome information better, but the searchability will be lower.

Fifthly, the mutation probability should be appropriately chosen because it can cause disturbance to the population. In this work, the selected mutation probability is 0.2.

Finally, the number of generations and stopping conditions must also be determined. If the number of generations is small, the calculation process will occur quickly, and vice versa. In this work, the number of generations selected is 1000. The optimal calculation program only stops when it has run for 1000 generations or 700 consecutive generations without the error exceeding the threshold value. The results illustrated in Figure 3b show the convergence of the fitness value after 1000 generations. The outstanding convergence ability of the algorithm causes the value of the fitness function to quickly decrease to zero.

After determining the optimal coefficients for the integrated controller, we obtain the PIDSMC-GA based control law. However, these parameters are only optimal under the specific condition mentioned in the algorithm's derivation. The system's quality may degrade if uncertain external

stimuli are not considered in optimizing the control coefficients. In addition, the influence of disturbances (road reaction torque) also changes continuously and dramatically affects the system's performance. Finally, the amplitude and frequency of the reference value also change in different cases leading to an increase in the tracking error. Therefore, it is necessary to flexibly adjust the controller's parameters to adapt to specific conditions. To solve this problem, we propose a fuzzy algorithm to flexibly fine-tune the optimal controller parameters. These parameters are adjusted for a range of values relative to the optimal value previously determined by GA, thus improving the overall quality of the control system. The combination of GA and fuzzy provides superior results in adjusting parameter values. This has been achieved by first calculating the optimal adjustment range using the GA instead of just choosing an arbitrary range empirically.

The fuzzy algorithm proposed in this research has three inputs. The first input is the road reaction torque, while the second and third inputs relate to the reference signals (amplitude  $A$  and frequency  $\omega$ ). Only the  $k_P$  and  $k_I$  coefficients are adjusted to improve the system's adaptability, while the  $k_D$  coefficient remains fixed (to reduce sensitivity's influence, the value of  $k_D$  should be small). The membership functions of the fuzzy system are shown in Figure 4 and Figure 5 corresponding to the coefficients  $k_P$  and  $k_I$  respectively. Looking at Figure 4, there are three types of membership functions used for the three inputs: GAUSSMF (Gaussian membership function), TRIMF (triangular membership function), and TRAPMF (trapezoidal membership function). For the  $k_I$  coefficient (Figure 5), TRIMF and TRAPMF functions are used. The mathematical model of the membership functions is given as follows:

GAUSSMF:

$$\mu_{MF}(x) = e^{-\frac{1}{2}\left(\frac{x-c}{\sigma}\right)^2} \quad (40)$$

TRIMF:

$$\mu_{MF}(x) = \begin{cases} 0 & x \leq a \\ \frac{x-a}{b-a} & a < x \leq b \\ \frac{c-x}{c-b} & b < x < c \\ 0 & x \geq c \end{cases} \quad (41)$$

TRAPMF:

$$\mu_{MF}(x) = \begin{cases} 0 & x \leq a \\ \frac{x-a}{b-a} & a < x \leq b \\ 1 & b < x \leq c \\ \frac{d-x}{d-c} & c < x < d \\ 0 & x \geq d \end{cases} \quad (42)$$

where  $a$ ,  $b$ ,  $c$ , and  $d$  are specific values of the membership function.

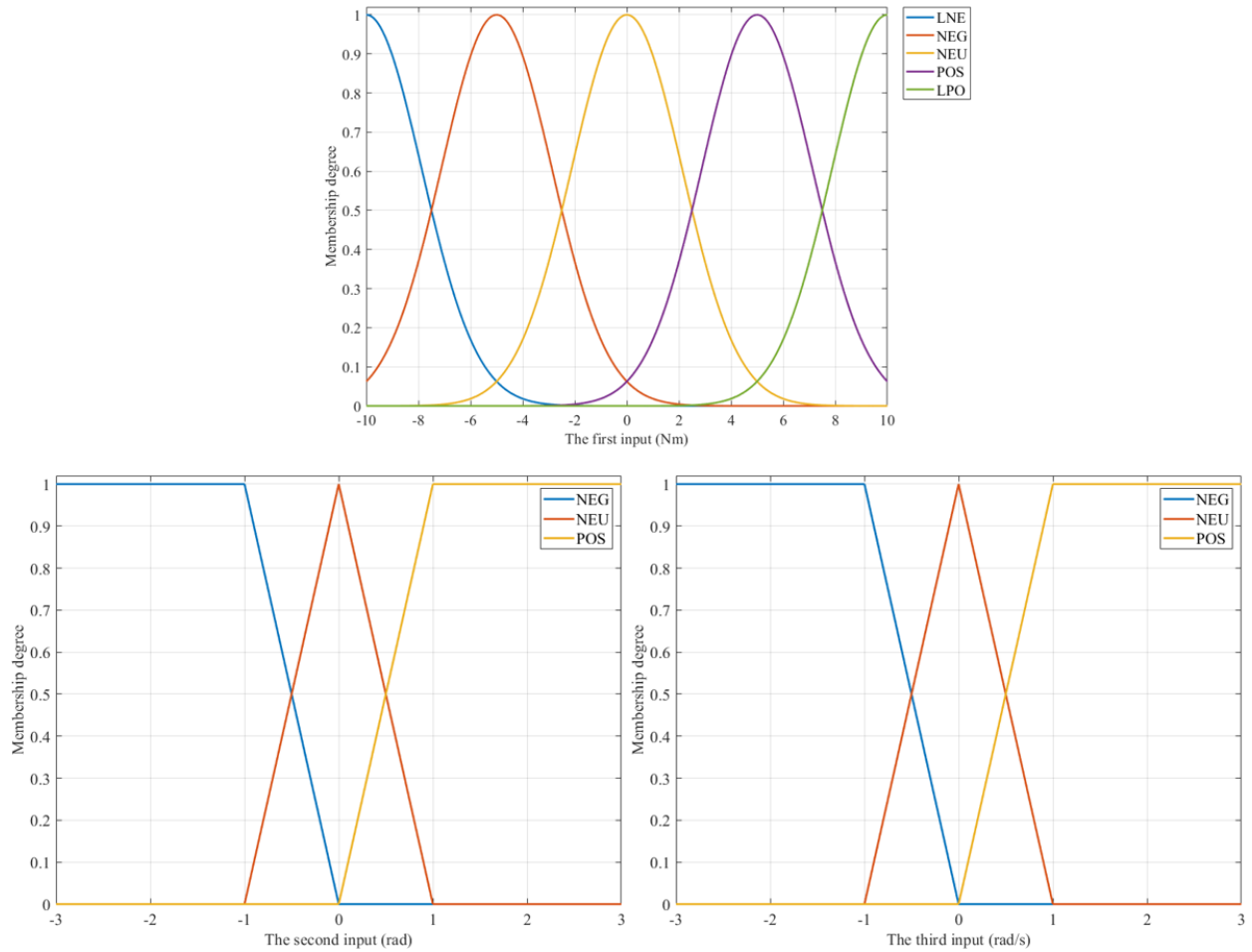


Figure 4. Membership functions of  $k_P$

The first input of the fuzzy algorithm for coefficient  $k_P$  has five membership functions (GAUSSMF) as shown in Figure 4. Unlike  $k_P$ , the first input of the fuzzy algorithm for  $k_I$  has seven membership functions (2 TRAPMF and 5 TRIMF) (Figure 5). These functions are divided into corresponding levels of the system, including VLN (very large negative), LNE (large negative), NEG (negative), NEU (neutral), POS (positive), LPO (large positive), and VLP (very large positive). The second and third inputs in Figure 4 and Figure 5 are similar. This is because the

influence of road reaction torque (the first input) is much more significant compared to the other factors.

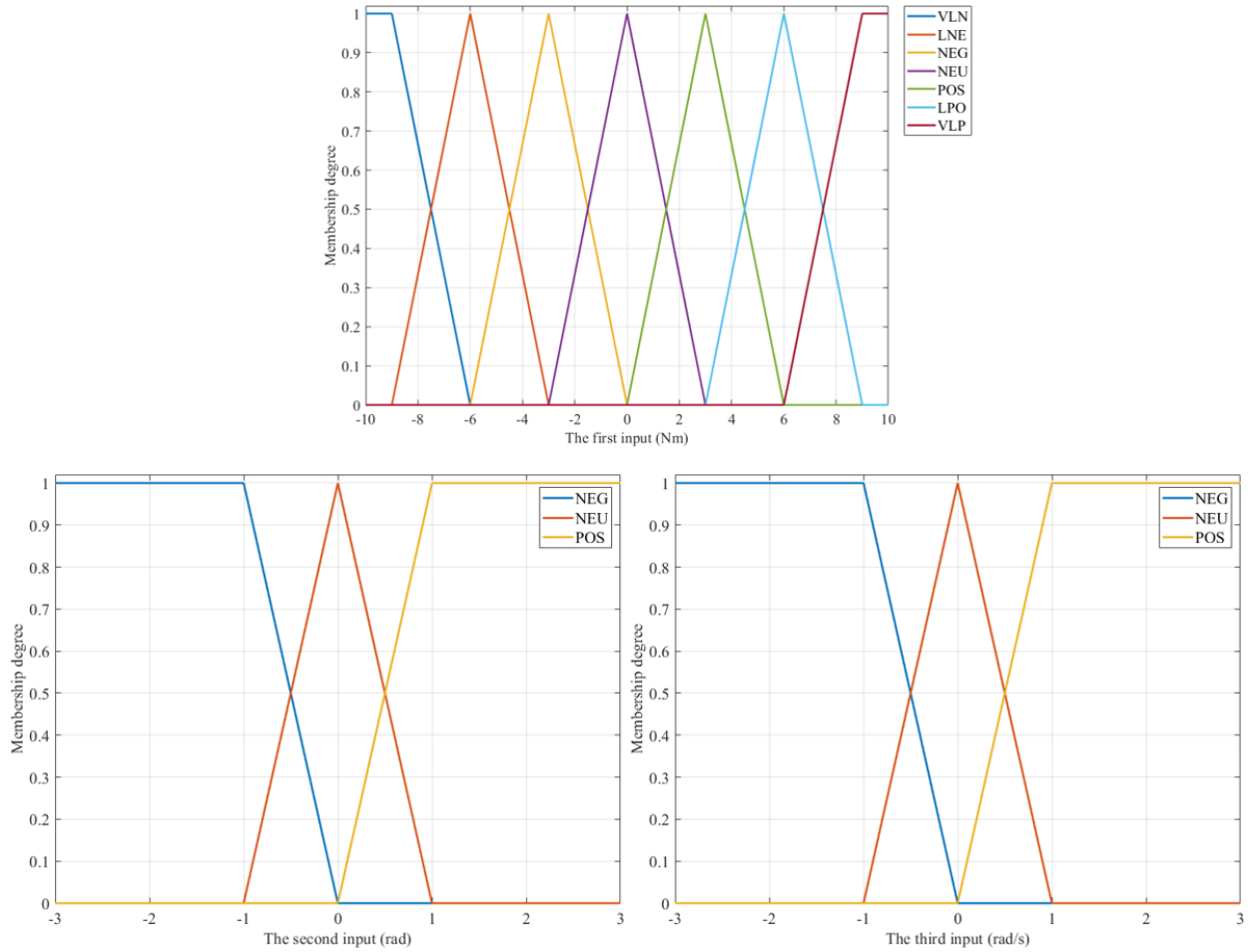


Figure 5. Membership functions of  $k_I$

Fuzzy surfaces are shown in Figure 6 (for the coefficient  $k_P$ ) and Figure 7 (for the coefficient  $k_I$ ). Fuzzy surfaces describe the relationship between inputs and outputs. The third input is represented through the internal links of the fuzzy surface. These surfaces are established based on fuzzy rules. Table 2 and Table 3 list the fuzzy rules used to adjust the values of the coefficients  $k_P$  and  $k_I$  respectively. The symbols for the output include ZE (zero), LO (low), NO (normal), HI (high), VH (very high), and EH (extremely high). In general, fuzzy rules and degrees of membership functions are often established based on the control designer's experience, which may be gained from previous simulations or experimentations.

Table 2. Fuzzy rules for the coefficient  $k_P$

<i>1<sup>st</sup> input</i>	<i>2<sup>nd</sup> input</i>	<i>3<sup>rd</sup> input</i>	<i>Output</i>	<i>1<sup>st</sup> input</i>	<i>2<sup>nd</sup> input</i>	<i>3<sup>rd</sup> input</i>	<i>Output</i>
LNE	NEG	NEG	VH	NEU	NEU	POS	LO
LNE	NEG	NEU	HI	NEU	POS	NEG	NO

LNE	NEG	PSO	VH	NEU	POS	NEU	LO
LNE	NEU	NEG	HI	NEU	POS	POS	NO
LNE	NEU	NEU	NO	POS	NEG	NEG	HI
LNE	NEU	PSO	HI	POS	NEG	NEU	NO
LNE	PSO	NEG	VH	POS	NEG	POS	HI
LNE	PSO	NEU	HI	POS	NEU	NEG	NO
LNE	PSO	PSO	VH	POS	NEU	NEU	LO
NEG	NEG	NEG	HI	POS	NEU	POS	NO
NEG	NEG	NEU	NO	POS	POS	NEG	HI
NEG	NEG	PSO	HI	POS	POS	NEU	NO
NEG	NEU	NEG	NO	POS	POS	POS	HI
NEG	NEU	NEU	LO	LPO	NEG	NEG	VH
NEG	NEU	PSO	NO	LPO	NEG	NEU	HI
NEG	PSO	NEG	HI	LPO	NEG	POS	VH
NEG	PSO	NEU	NO	LPO	NEU	NEG	HI
NEG	PSO	PSO	HI	LPO	NEU	NEU	NO
NEU	NEG	NEG	NO	LPO	NEU	POS	HI
NEU	NEG	NEU	LO	LPO	POS	NEG	VH
NEU	NEG	PSO	NO	LPO	POS	NEU	HI
NEU	NEU	NEG	LO	LPO	POS	POS	VH
NEU	NEU	NEU	ZE				

Table 3. Fuzzy rules for the coefficient  $k_I$

<i>1<sup>st</sup> input</i>	<i>2<sup>nd</sup> input</i>	<i>3<sup>rd</sup> input</i>	<i>Output</i>	<i>1<sup>st</sup> input</i>	<i>2<sup>nd</sup> input</i>	<i>3<sup>rd</sup> input</i>	<i>Output</i>
VLN	NEG	NEG	EH	NEU	NEU	POS	LO
VLN	NEG	NEU	VH	NEU	POS	NEG	NO
VLN	NEG	POS	EH	NEU	POS	NEU	LO
VLN	NEU	NEG	VH	NEU	POS	POS	NO
VLN	NEU	NEU	HI	POS	NEG	NEG	HI
VLN	NEU	POS	VH	POS	NEG	NEU	NO
VLN	POS	NEG	EH	POS	NEG	POS	HI
VLN	POS	NEU	VH	POS	NEU	NEG	NO
VLN	POS	POS	EH	POS	NEU	NEU	LO
LNE	NEG	NEG	VH	POS	NEU	POS	NO
LNE	NEG	NEU	HI	POS	POS	NEG	HI
LNE	NEG	POS	VH	POS	POS	NEU	NO
LNE	NEU	NEG	HI	POS	POS	POS	HI
LNE	NEU	NEU	NO	LPO	NEG	NEG	VH
LNE	NEU	POS	HI	LPO	NEG	NEU	HI
LNE	POS	NEG	VH	LPO	NEG	POS	VH
LNE	POS	NEU	HI	LPO	NEU	NEG	HI
LNE	POS	POS	VH	LPO	NEU	NEU	NO
NEG	NEG	NEG	HI	LPO	NEU	POS	HI
NEG	NEG	NEU	NO	LPO	POS	NEG	VH

NEG	NEG	POS	HI	LPO	POS	NEU	HI
NEG	NEU	NEG	NO	LPO	POS	POS	VH
NEG	NEU	NEU	LO	VLP	NEG	NEG	EH
NEG	NEU	POS	NO	VLP	NEG	NEU	VH
NEG	POS	NEG	HI	VLP	NEG	POS	EH
NEG	POS	NEU	NO	VLP	NEU	NEG	VH
NEG	POS	POS	HI	VLP	NEU	NEU	HI
NEU	NEG	NEG	NO	VLP	NEU	POS	VH
NEU	NEG	NEU	LO	VLP	POS	NEG	EH
NEU	NEG	POS	NO	VLP	POS	NEU	VH
NEU	NEU	NEG	LO	VLP	POS	POS	EH
NEU	NEU	NEU	ZE				

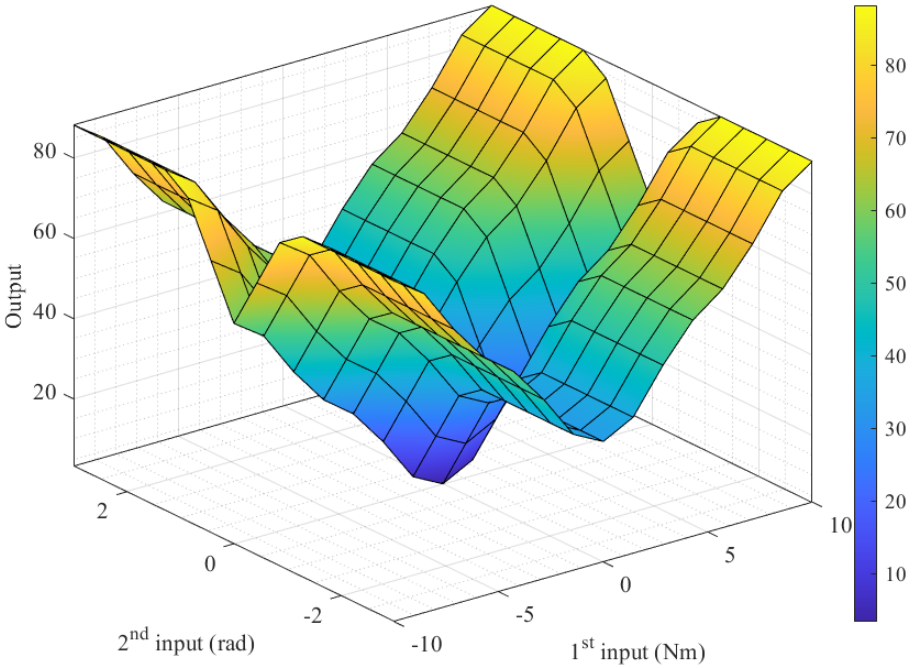


Figure 6. Fuzzy surface for the coefficient  $k_P$

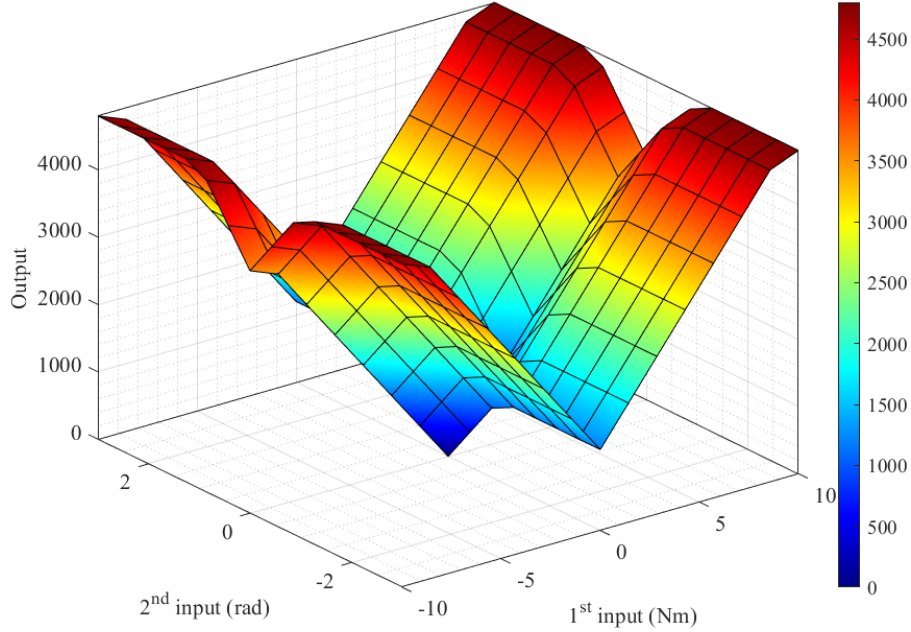


Figure 7. Fuzzy surface for the coefficient  $k_t$

### 3. Results

Numerical computations and simulations were performed in the MATLAB-Simulink environment. This process was performed by a PC system with the following technical configuration: CPU i9-12900K, 32 GB of RAM, and a 512 GB SSD.

#### 3.1. Conditions

The parameters of the EPS system are shown in Table 4. These values are referred in [44]. The input to the simulation setup is road reaction torque ( $T_r$ ). There are three cases shown in Figures 8, 9, and 10. The magnitude of  $T_r$  is varied considering four scenarios: (a)  $T_r = 2$  Nm, (b)  $T_r = 4$  Nm, (c)  $T_r = 6$  Nm, and (d)  $T_r = 8$  Nm. The reference signal is categorized into two types corresponding to two conditions ( $A = 1$  rad,  $\omega = 1$  rad/s and  $A = 2$  rad,  $\omega = 2$  rad/s). The outputs from the simulation setup are the change in motor angle, steering column angle, and current. These results are evaluated based on the error between the actual signal and the desired signal.

Table 4. Electric steering specifications

Symbol	Value	Unit	Symbol	Value	Unit
$I_c$	0.04	kgm <sup>2</sup>	$K_t$	0.05	NmA <sup>-1</sup>
$I_m$	0.0004	kgm <sup>2</sup>	$N$	13.65	-
$B_c$	0.072	Nmsrad <sup>-1</sup>	$R_m$	0.37	$\Omega$
$B_m$	0.0032	Nmsrad <sup>-1</sup>	$r_p$	0.007	m
$B_r$	3820	Nsrad <sup>-1</sup> m <sup>-1</sup>	$M_r$	32	kg
$K_c$	115	Nmrad <sup>-1</sup>	$L_m$	0.0056	H
$K_r$	43000	Nrad <sup>-1</sup> m <sup>-1</sup>			

In each scenario, we used two simulation situations as detailed below:

+ The first situation: The EPS system is controlled by the optimal and integrated algorithm (PIDSMC-GA). The controller parameters are optimized by GA and do not change under the investigated conditions.

+ The second situation: The EPS system is controlled by the intelligent, optimal and integrated algorithm (FPIDSMC-GA). The controller parameters are dynamically fine-tuned based on previously defined optimal values. This helps to improve the system's adaptability to different conditions.

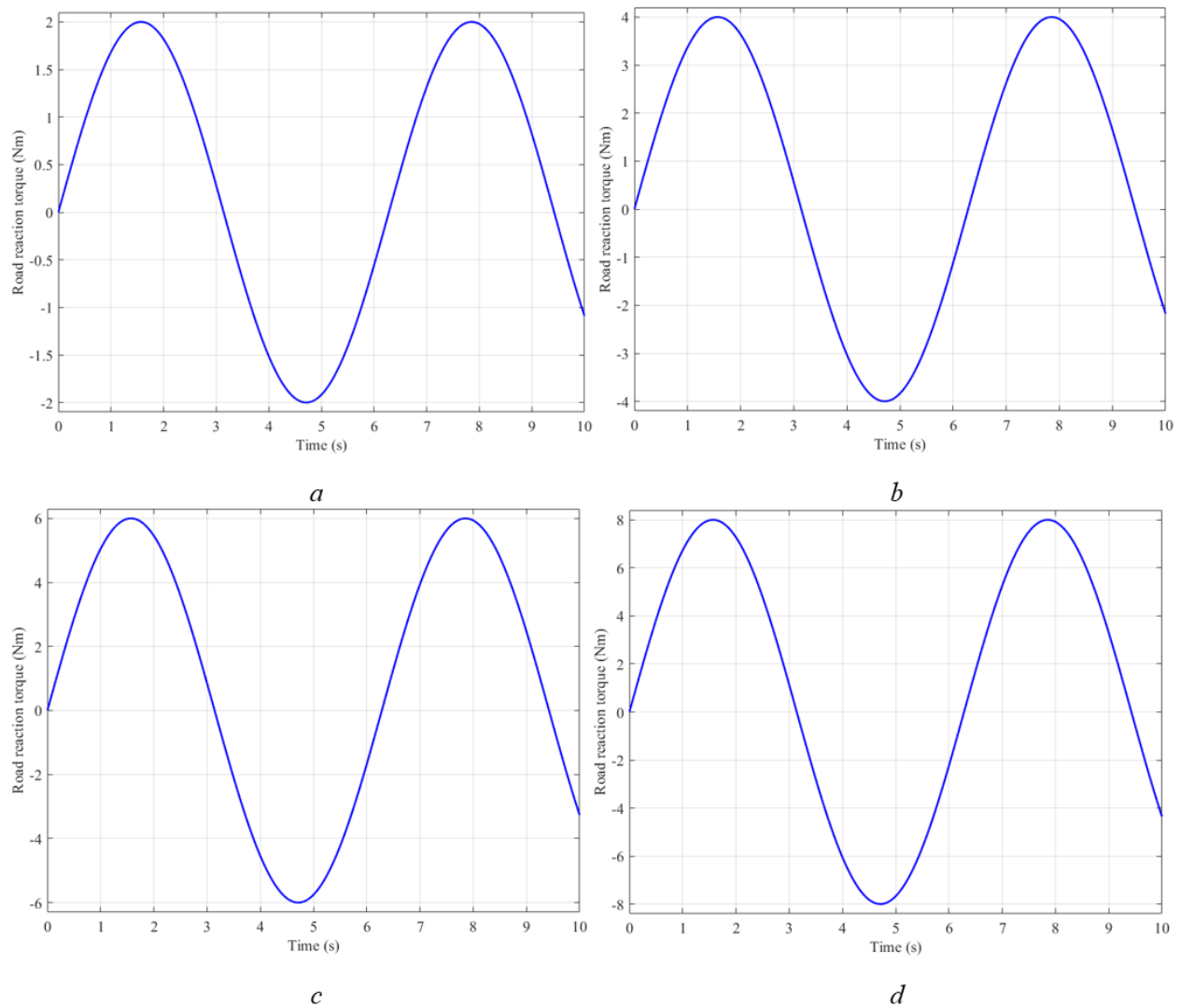


Figure 8. Road reaction torque – 1<sup>st</sup> case

(a)  $T_r = 2$  Nm, (b)  $T_r = 4$  Nm, (c)  $T_r = 6$  Nm, (d)  $T_r = 8$  Nm

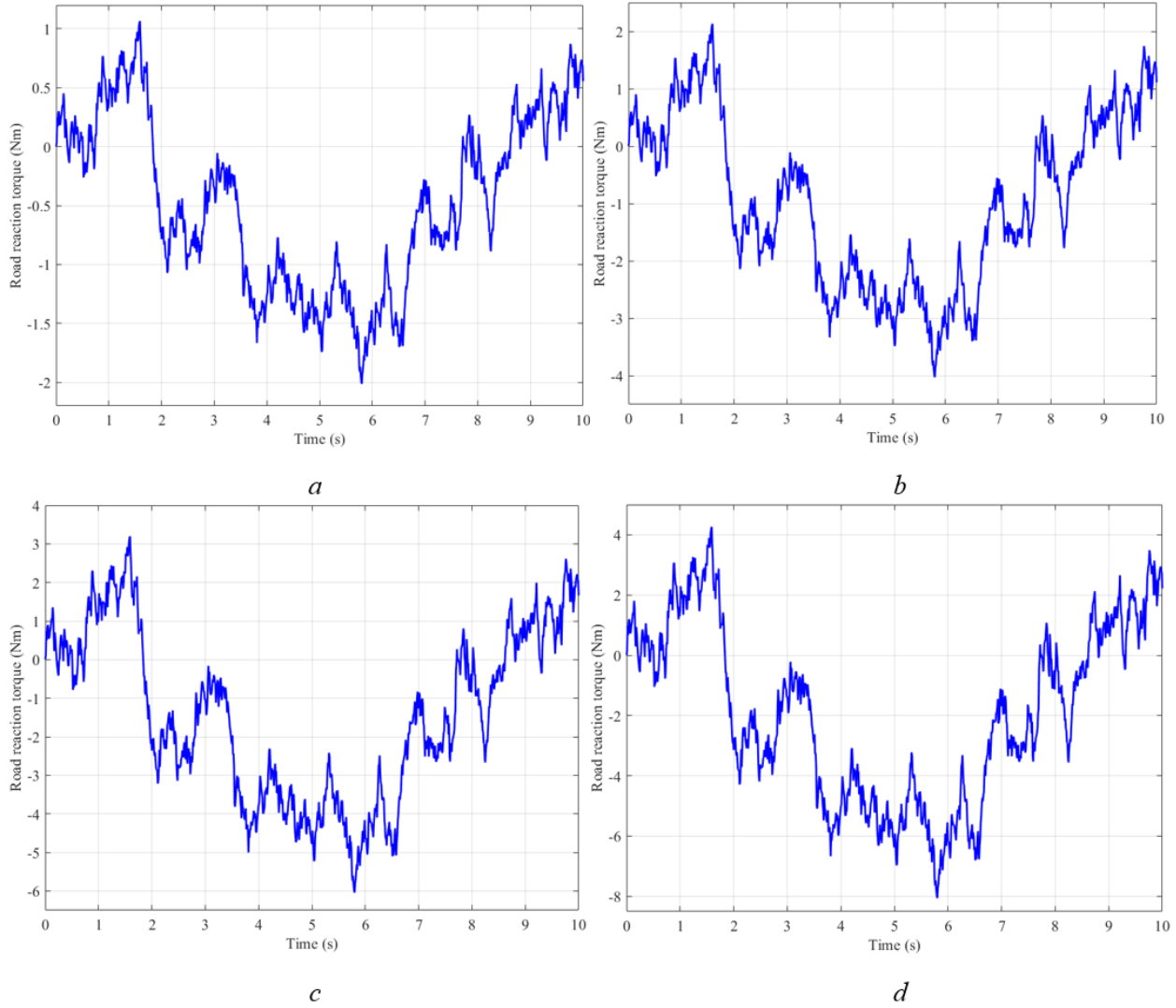


Figure 9. Road reaction torque – 2<sup>nd</sup> case

(a)  $T_r = 2$  Nm, (b)  $T_r = 4$  Nm, (c)  $T_r = 6$  Nm, (d)  $T_r = 8$  Nm

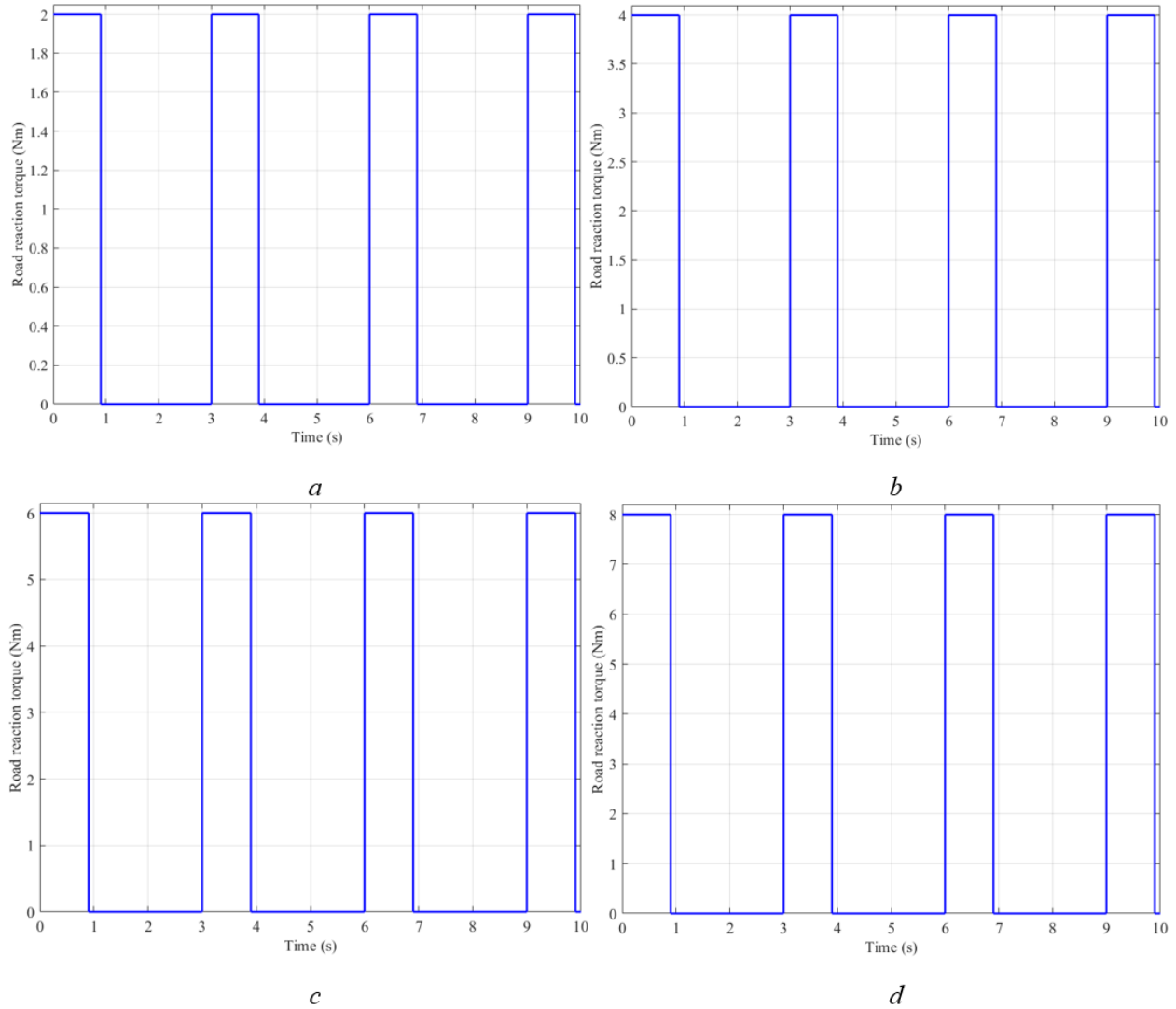


Figure 10. Road reaction torque – 3<sup>rd</sup> case

(a)  $T_r = 2$  Nm, (b)  $T_r = 4$  Nm, (c)  $T_r = 6$  Nm, (d)  $T_r = 8$  Nm

### 3.2. Simulation results

#### 3.2.1. The first condition ( $A = 1$ rad, $\omega = 1$ rad/s)

The reference signal for the motor angle is a periodic sinusoidal. Three cases are investigated under this condition, corresponding to the road reaction torques.

#### The first case:

The first case refers to the use of road disturbance in the form of a periodic sinusoidal function (Figure 8). This case has four scenarios corresponding to four levels of stimulation from the road surface. Therefore, the simulation results are illustrated as figures with four corresponding subplots.

Figure 11 depicts the change in motor angle throughout the simulation time (10s). In the first scenario, the PIDSMC-GA and FPIDSMC-GA signals closely track the reference signal (Figure 11a). The maximum error in the motor angle is found to be  $0.24^\circ$  for the situation applying the PIDSMC-GA. This is further reduced to  $0.19^\circ$  in case of applying the FPIDSMC-GA. Additionally, the value of the average error calculated according to the RMS criterion is also very small, which is  $0.09^\circ$  and  $0.04^\circ$  in case of PIDSMC-GA and FPIDSMC-GA respectively. In the second scenario, control signals follow the desired signal as illustrated in Figure 11b. For the PIDSMC-GA, the error reaches up to  $0.30^\circ$ . When the FPIDSMC-GA controls the EPS system, the error between the reference signal and the actual output obtained is minimal and is only  $0.19^\circ$ , which is similar to the first scenario. Looking at the RMS value, we notice that the average error does not change for the FPIDSMC-GA situation, while this figure increases by  $0.05^\circ$  for the other situation.

In the following two scenarios ( $T_r = 6 \text{ Nm}$  and  $T_r = 8 \text{ Nm}$ ), the value of the motor angle follows the desired value. The error between scenarios is almost unchanged when using the optimal integrated fuzzy algorithm (see Table 5). For the PIDSMC-GA, the error value increases as the road disturbance increases, but the change is relatively small. The amplitude of the reference signal is  $1 \text{ rad} \approx 57.32^\circ$ , while the maximum error between the output signal and the reference signal is only  $1.06^\circ$ . In general, both algorithms proposed in this research can guarantee the system's stability in the first case.

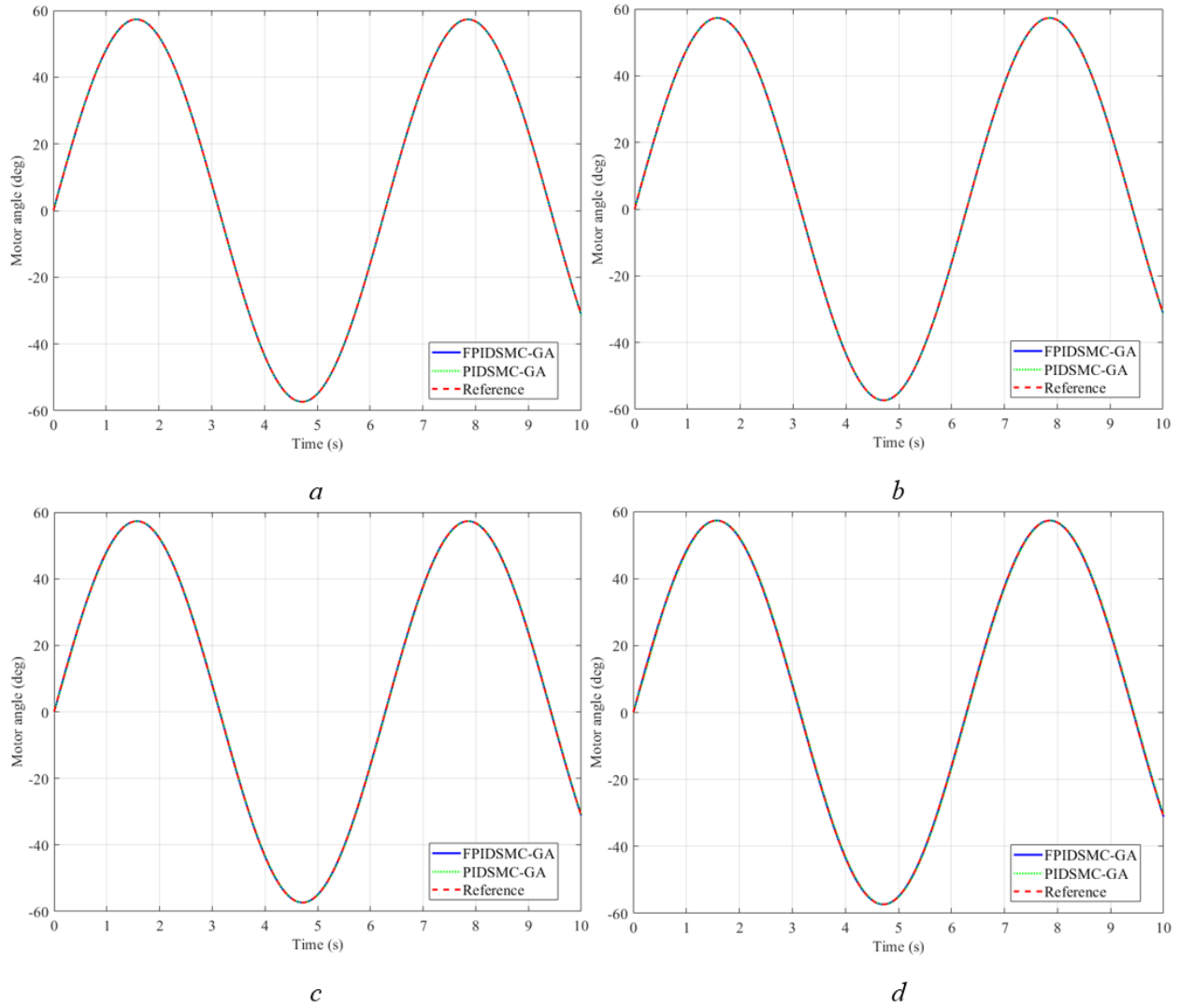


Figure 11. Motor angle – The first case

(a)  $T_r = 2$  Nm, (b)  $T_r = 4$  Nm, (c)  $T_r = 6$  Nm, (d)  $T_r = 8$  Nm

In addition to monitoring the motor angle, the change in steering column angle has also been considered carefully. The value of the steering column angle is much smaller than the motor angle. Looking at Figure 12 closer, we can see that the trend in change of the steering column angle is similar to that of the motor angle. The output signals follow the set reference signal, even though the road reaction torque changes from  $T_r = 2$  Nm to  $T_r = 8$  Nm. Simulation results demonstrate that the maximum error in the steering column reaches up to  $0.12^\circ$  (for all the four scenarios) when the FPIDSMC-GA based control law is applied to control the EPS system. The difference in the average errors attained by PIDSMC-GA and FPIDSMC-GA is negligible.

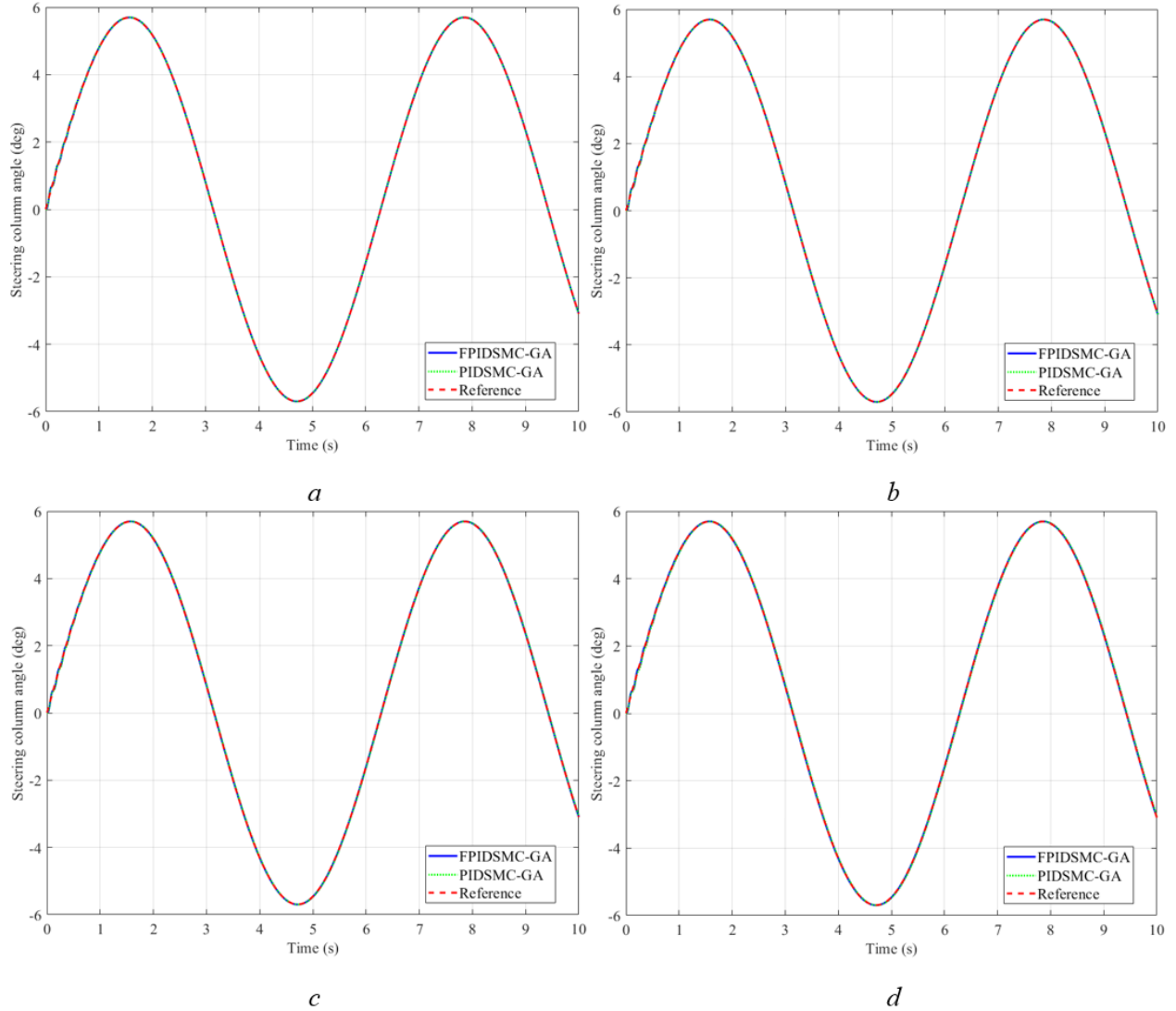


Figure 12. Steering column angle – The first case

(a)  $T_r = 2$  Nm, (b)  $T_r = 4$  Nm, (c)  $T_r = 6$  Nm, (d)  $T_r = 8$  Nm

Compared with HPS systems, EPS systems consume less energy. We have considered the energy consumption in an EPS system in simulation cases. Figure 13 depicts the change in current in different scenarios. According to the research findings, the maximum and average values of the current demonstrated by both PIDSMC-GA and FPIDSMC-GA are same. In the first and second scenarios, the current value is quite small. This number increases twofold as the road disturbance increases up to 6 Nm, and it continues to rise with the increase in the value of  $T_r$ .

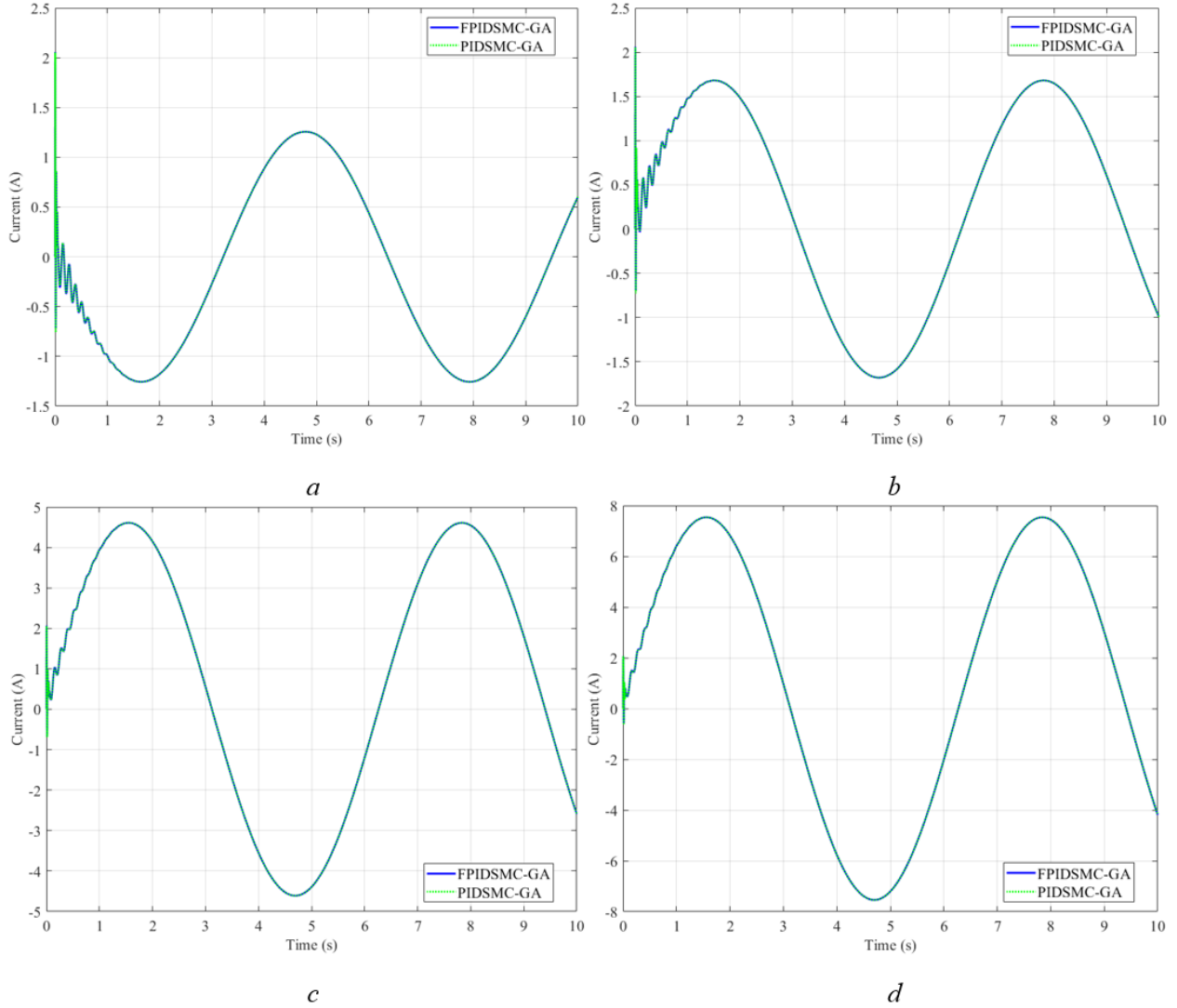


Figure 13. Current – The first case

(a)  $T_r = 2$  Nm, (b)  $T_r = 4$  Nm, (c)  $T_r = 6$  Nm, (d)  $T_r = 8$  Nm

In the first case, system stability is guaranteed in all scenarios when we used either of the two control algorithms proposed in this research. In the following, higher-frequency road excitation is used to investigate the system's stability.

Table 5. Simulation results (1<sup>st</sup> case – 1<sup>st</sup> condition)

	FPIDSMC-GA				PIDSMC-GA			
$T_r$ (Nm)	2	4	6	8	2	4	6	8
Error $\psi_{m\_max}$ (°)	0.19	0.19	0.19	0.20	0.24	0.30	0.66	1.06

<i>Error</i> $\psi_{m\_RMS} (^\circ)$	0.04	0.04	0.05	0.07	0.09	0.14	0.34	0.53
<i>Error</i> $\psi_{c\_max} (^\circ)$	0.12	0.12	0.12	0.12	0.12	0.12	0.13	0.13
<i>Error</i> $\psi_{c\_RMS} (^\circ)$	0.02	0.02	0.02	0.02	0.03	0.03	0.03	0.04
<i>Value</i> $i_{m\_max} (A)$	2.06	2.06	4.61	7.54	2.05	2.06	4.61	7.54
<i>Value</i> $i_{m\_RMS} (A)$	0.78	1.10	3.01	4.96	0.78	1.10	3.01	4.96

### The second case:

Random road disturbances are used in the second case (Figure 9). The simulation results included motor angle, steering column angle and current. The change in motor angle is depicted by the subplots in Figure 14. In the first scenario ( $T_r = 2$  Nm), the output signals from both control laws follow the reference signal (Figure 14a). The maximum errors in case of PIDSMC-GA and FPIDSMC-GA are  $1.17^\circ$  and  $0.32^\circ$  respectively, while the corresponding RMS errors are  $0.45^\circ$  and  $0.11^\circ$ . Once the value of road disturbance increases, the difference between these values becomes larger. In the second scenario ( $T_r = 4$  Nm), the maximum error between the output signal and the reference signal when using the PIDSMC-GA and FPIDSMC-GA is  $2.00^\circ$  and  $0.55^\circ$ . The average error value is decreased to  $0.19^\circ$  by applying FPIDSMC-GA control law compared to PIDSMC-GA (where it is  $0.81^\circ$  as illustrated in Figure 14b).

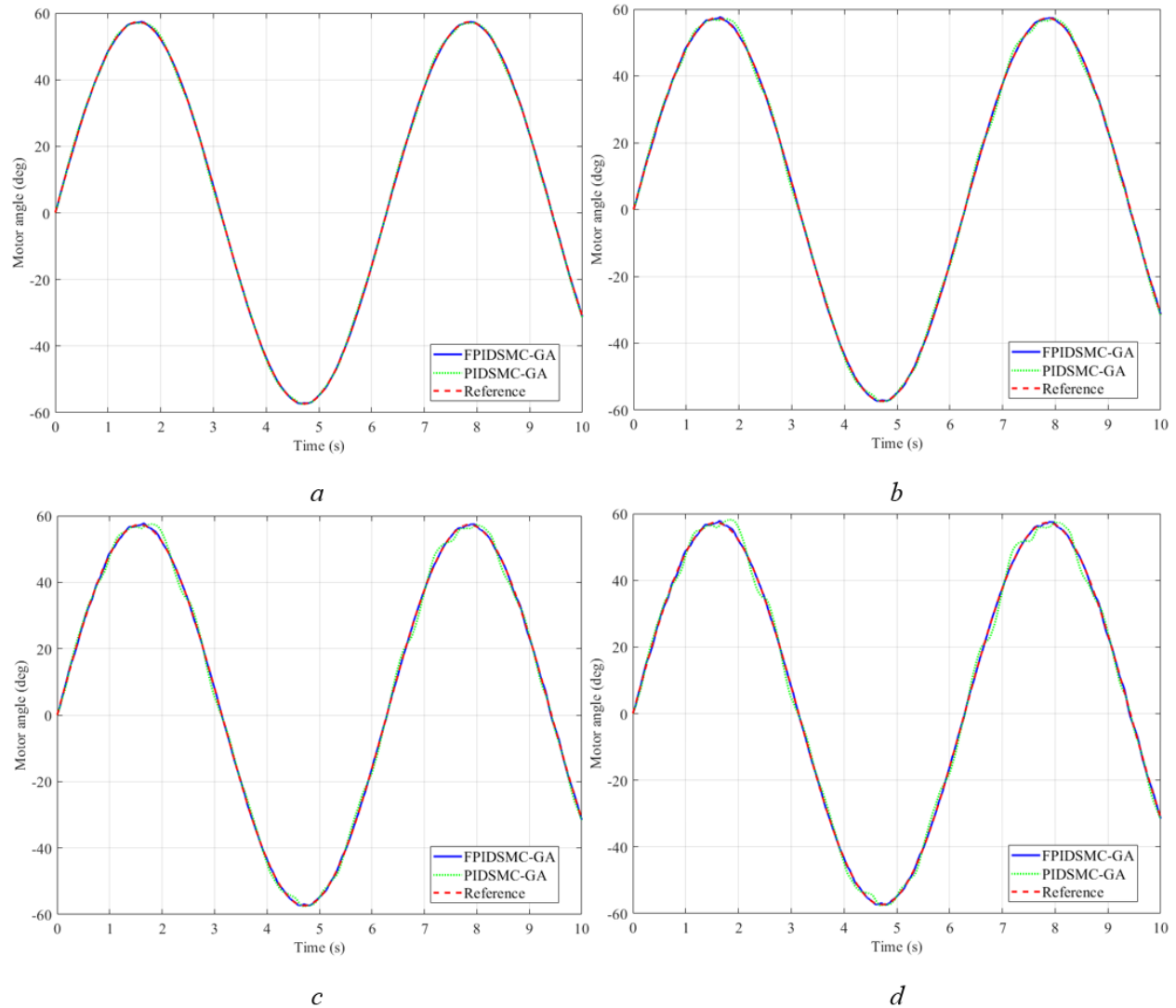


Figure 14. Motor angle – The second case

(a)  $T_r = 2$  Nm, (b)  $T_r = 4$  Nm, (c)  $T_r = 6$  Nm, (d)  $T_r = 8$  Nm

Looking at Figure 14c more closely, we can see a difference between the output signal and the desired signal in case of PIDSMC-GA. According to the simulation results, the maximum error in this case goes up to  $3.01^\circ$ , while the average error is  $1.19^\circ$ . Compared to the first case, this error increases by 4.5 times as illustrated in Figure 14c. This indicates that the optimal parameters of the controller are only suitable for specific conditions. When these conditions change, the control performance and so as the quality of the system can be affected. However, the impact in this scenario is not significant. If the parameters of the optimal controller are dynamically adjusted by the fuzzy algorithm, the system's response is more efficient. The output signal obtained from the FPIDSMC-GA controller follows the reference signal (Figure 14c). The difference between the performance achieved by FPIDSMC-GA and reference is inconsiderable and is  $0.76^\circ$  (maximum value) and  $0.27^\circ$  (average value).

The final scenario shows the system's stability under the most severe conditions ( $T_r = 8$  Nm). There is a significant difference between the results obtained from the PIDSMC-GA and FPIDSMC-GA based control laws. In case of  $e$  the PIDSMC-GA controller, the system's response is not sustainable. The value of the error can reach up to  $4.05^\circ$  With the average error reaching  $1.55^\circ$  calculated according to the RMS criterion. On the contrary, the value of the motor angle follows the reference signal at all times in case of FPIDSMC-GA (Figure 14d). Therefore, their error values are minor,  $0.97^\circ$  (maximum) and  $0.33^\circ$  (average). These error values are 4.18 time and 4.70 time lower than the corresponding values achieved earlier in case of the PIDSMC-GA controller. This difference in errors between the two control laws demonstrate over-performance of FPIDSMC-GA based controller compared to PIDSMC-GA control law.

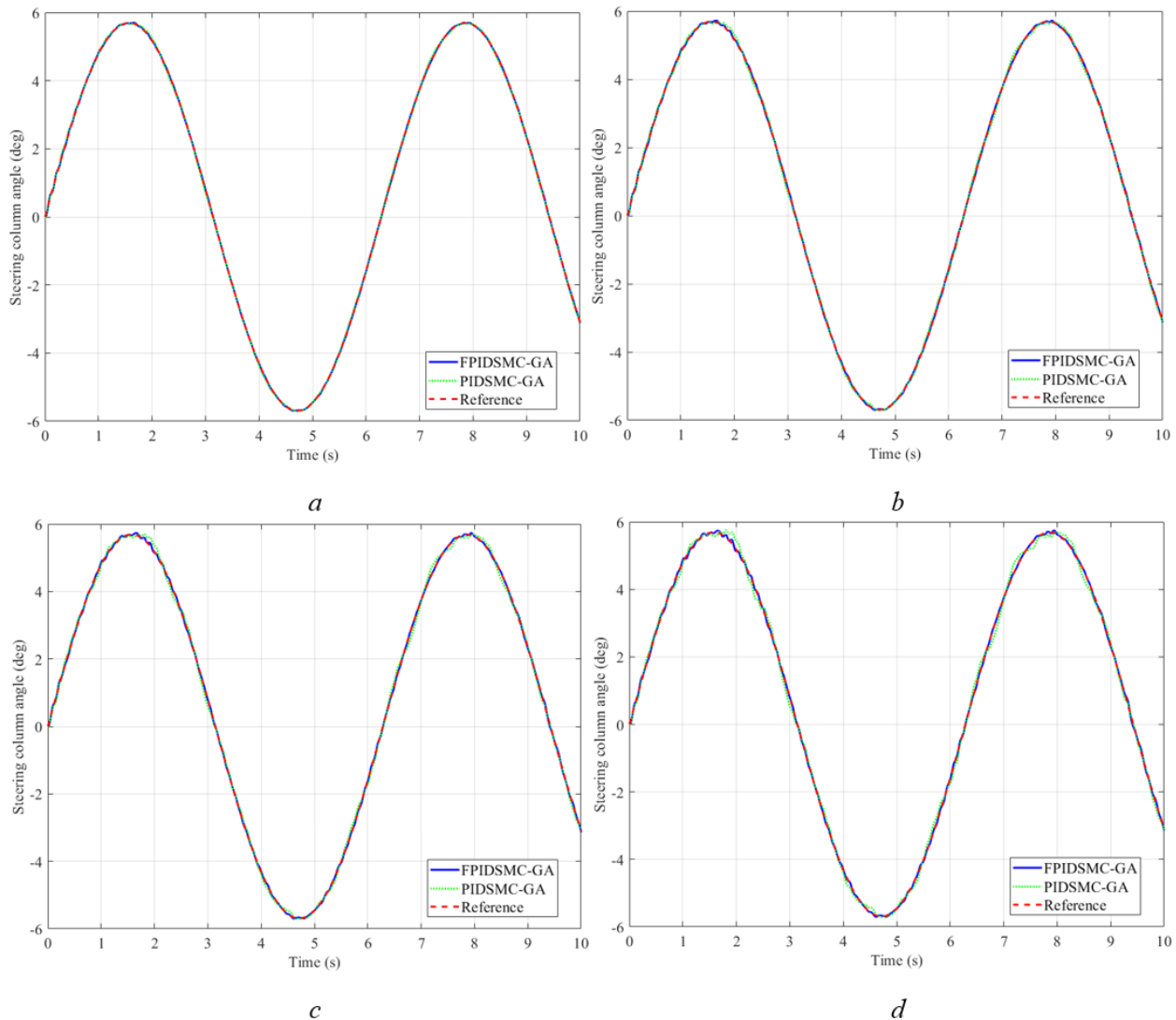


Figure 15. Steering column angle – The second case

(a)  $T_r = 2$  Nm, (b)  $T_r = 4$  Nm, (c)  $T_r = 6$  Nm, (d)  $T_r = 8$  Nm

The trend in change of steering column angle is similar to that of motor angle. Figure 15 shows that the output signal followed the reference signal in the first scenario (Figure 15a) as well as in the second scenario (Figure 15b). If road disturbance increases, the results achieved from the PIDSMC-GA controller cannot precisely follow the reference signal (Figure 15c). The output signal obtained deviates from the reference signal when the road reaction torque increases as shown in Figure 15d. According to simulation results, the maximum error of the steering column angle is  $0.35^\circ$  when we use the PIDSMC-GA to control the EPS system. Application of the FPIDSMC-GA permits reducing the maximum error as well as the average error by a factor of three, which is a significant improvement in achieving better control performance. Table 6 presents the corresponding results of the second case with first condition.

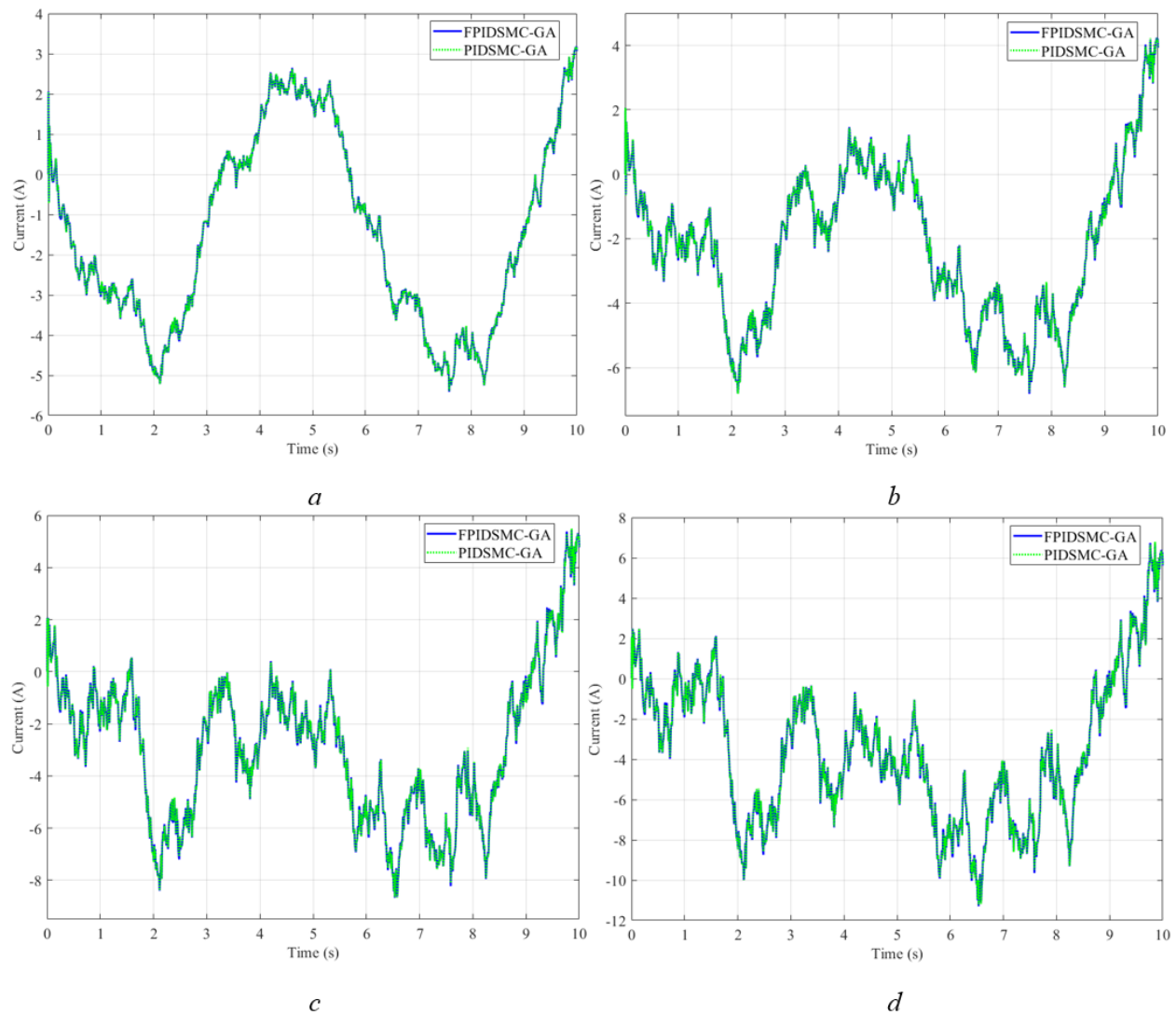


Figure 16. Current – The second case

(a)  $T_r = 2$  Nm, (b)  $T_r = 4$  Nm, (c)  $T_r = 6$  Nm, (d)  $T_r = 8$  Nm

Figure 16 illustrates the energy consumption when using electric steering in different scenarios. If the value of  $T_r$  is increased, the control current also increases. The maximum value of  $i_m$  can be up to 11.29A corresponding to  $T_r = 8$  Nm (Figure 16d). The difference between two signals received from the two controllers (FPIDSMC-GA and PIDSMC-GA) under discussion is insignificant.

Table 6. Simulation results (2<sup>nd</sup> case – 1<sup>st</sup> condition)

	FPIDSMC-GA				PIDSMC-GA			
$T_r$ (Nm)	2	4	6	8	2	4	6	8
<i>Error</i> $\psi_{m\_max}$ (°)	0.32	0.55	0.76	0.97	1.17	2.00	3.01	4.05
<i>Error</i> $\psi_{m\_RMS}$ (°)	0.11	0.19	0.27	0.33	0.45	0.81	1.19	1.55
<i>Error</i> $\psi_{c\_max}$ (°)	0.12	0.12	0.12	0.12	0.12	0.17	0.26	0.35
<i>Error</i> $\psi_{c\_RMS}$ (°)	0.02	0.02	0.03	0.04	0.04	0.06	0.09	0.12
<i>Value</i> $i_{m\_max}$ (A)	5.41	6.81	8.67	11.29	5.38	6.81	8.66	11.22
<i>Value</i> $i_{m\_RMS}$ (A)	2.93	3.28	3.90	4.66	2.93	3.28	3.91	4.67

**The third case:**

The third case represents and simulates a more extreme condition. Here, the excitation signal from the road surface has a rectangular pulse (Figure 10). The value of this signal increases rapidly from zero to peak and thus, it is a suitable signal to analyze stability of the steering system.

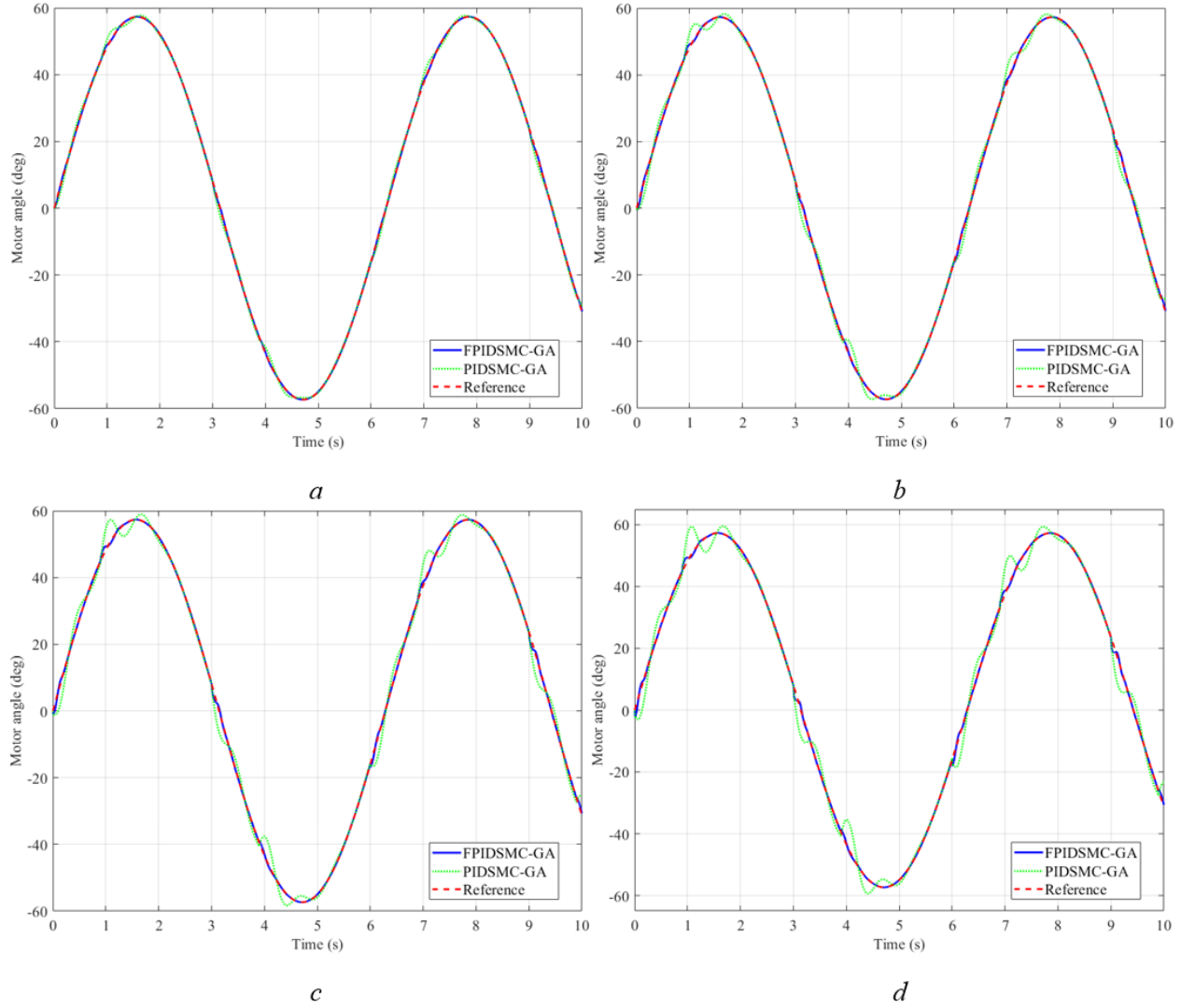


Figure 17. Motor angle – The third case

(a)  $T_r = 2$  Nm, (b)  $T_r = 4$  Nm, (c)  $T_r = 6$  Nm, (d)  $T_r = 8$  Nm

In the first case (Figure 11a) and the second case (Figure 14a), both output signals obtained from the two controllers follow the reference signal. This is not true in the third case. If we apply the PIDSMC-GA optimization algorithm to the EPS system, the error between the output signal and the desired signal turns out to be  $2.53^\circ$  for the first scenario (Figure 17a). However, application of FPIDSMC-GA permits having better trajectory tracking with a maximum error of no more than  $1^\circ$ . In the second scenario ( $T_r = 4$  Nm), the error between the output signal obtained from the controllers and the reference signal increases. The maximum values of errors are  $4.78^\circ$  and  $1.63^\circ$  for the PIDSMC-GA and FPIDSMC-GA situations respectively (Figure 17b).

A more considerable difference can be seen in the third scenario. According to Figure 17c, the value obtained from the PIDSMC-GA fluctuates around the reference value at times corresponding to the excitation pulse from the road surface. Consequently, the maximum value of error can be as

high as  $7.05^\circ$  while the RMS error is  $2.40^\circ$ . However, the output signal obtained from the FPIDSMC-GA controller still closely follows the desired signal. At some point, this signal may fluctuate slightly but not significantly. According to the results illustrated in Figure 17c, the maximum error in FPIDSMC-GA is only  $2.26^\circ$ , which is 32.06% compared to the situation where only the PIDSMC-GA controller is applied. This over-performance of FPIDSMC-GA is primarily due to the flexible adjustment of controller parameters based on the fuzzy algorithm. System responsiveness and stability are guaranteed under many different conditions.

In the last scenario ( $T_r = 8 \text{ Nm}$ ), the difference between the desired and actual values increases rapidly if the controller parameters are not dynamically tuned. Figure 17d shows that the output signal obtained from PIDSMC-GA does not adequately track the reference signal. The maximum value of the error can be up to  $9.41^\circ$ , which is 16.42% of the oscillation amplitude of the desired signal. Application of the fuzzy algorithm to adjust the controller's parameters to adapt well to different conditions improves the control performance. This situation results in a maximum error value of  $3.32^\circ$  only, which is 35.28% of the situation corresponding to PIDSMC-GA. The value of the RMS error when PIDSMC-GA is applied is  $3.25^\circ$ , which does not exceed  $1^\circ$  in the situation with the FPIDSMC-GA. These results establish the superiority of combining the fuzzy algorithm with the PIDSMC-GA optimization algorithm proposed in the present research. Some recent studies [29, 44, 52] illustrate that the output signal can be affected by road disturbances.

Figure 18 gives information about the change in steering column angle over time. In the first scenario, the signal difference is insignificant (Figure 18a). In the second scenario, the error between the output signal and the desired setpoint is evident for the PIDSMC-GA situation. The excitation pulse from road disturbance increases the error (Figure 18b). In the third scenario, the signal obtained from the PIDSMC-GA fluctuates around the set signal with a maximum and average errors of  $0.55^\circ$  and  $0.18^\circ$  respectively. In contrast, when applying the FPIDSMC-GA based control law, the output signal still closely follows the reference signal with minor errors (max =  $0.28^\circ$  and RMS =  $0.06^\circ$ ). Figure 18d shows that the difference between the results is largest when  $T_r = 8 \text{ Nm}$ . According to this finding, the maximum value of the error can reach up to  $0.75^\circ$  with the control based on PIDSMC-GA. However, the system's stability is guaranteed once we apply the intelligent adaptive algorithm (FPIDSMC-GA) to control the EPS system. Based on the ability to flexibly fine-tune the controller's parameters, the FPIDSMC-GA can potentially help to improve the system stability and adaptability under more severe conditions.

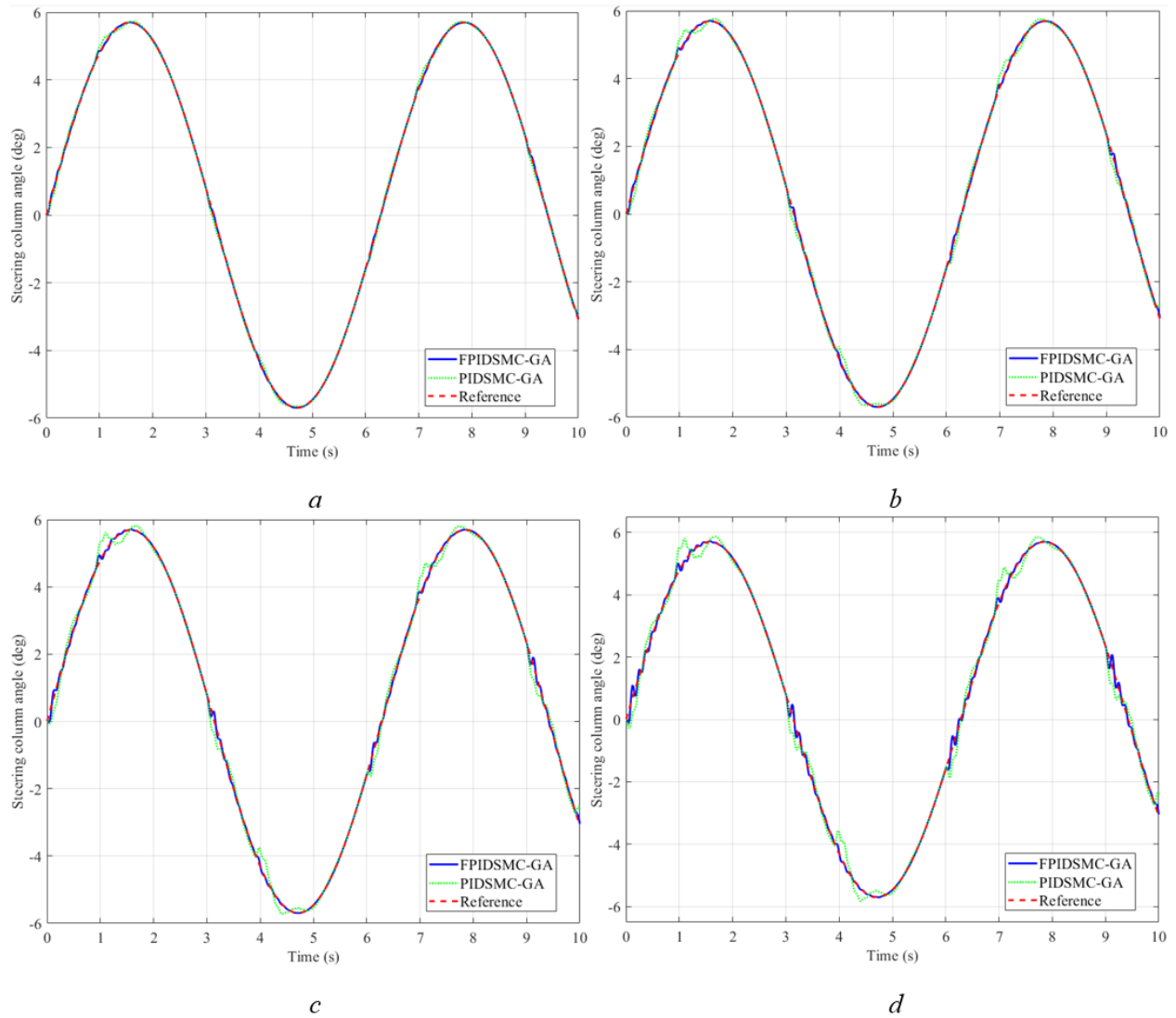


Figure 18. Steering column angle – The third case

(a)  $T_r = 2$  Nm, (b)  $T_r = 4$  Nm, (c)  $T_r = 6$  Nm, (d)  $T_r = 8$  Nm

According to Figure 19, the change in the current signal in both situations is similar. In general, the peak value in FPIDSMC-GA is slightly higher than the corresponding value in PIDSMC-GA, but the average value calculated according to the RMS criterion is equivalent in both control algorithms thus indicating same average energy consumption. These results can be seen in Table 7.

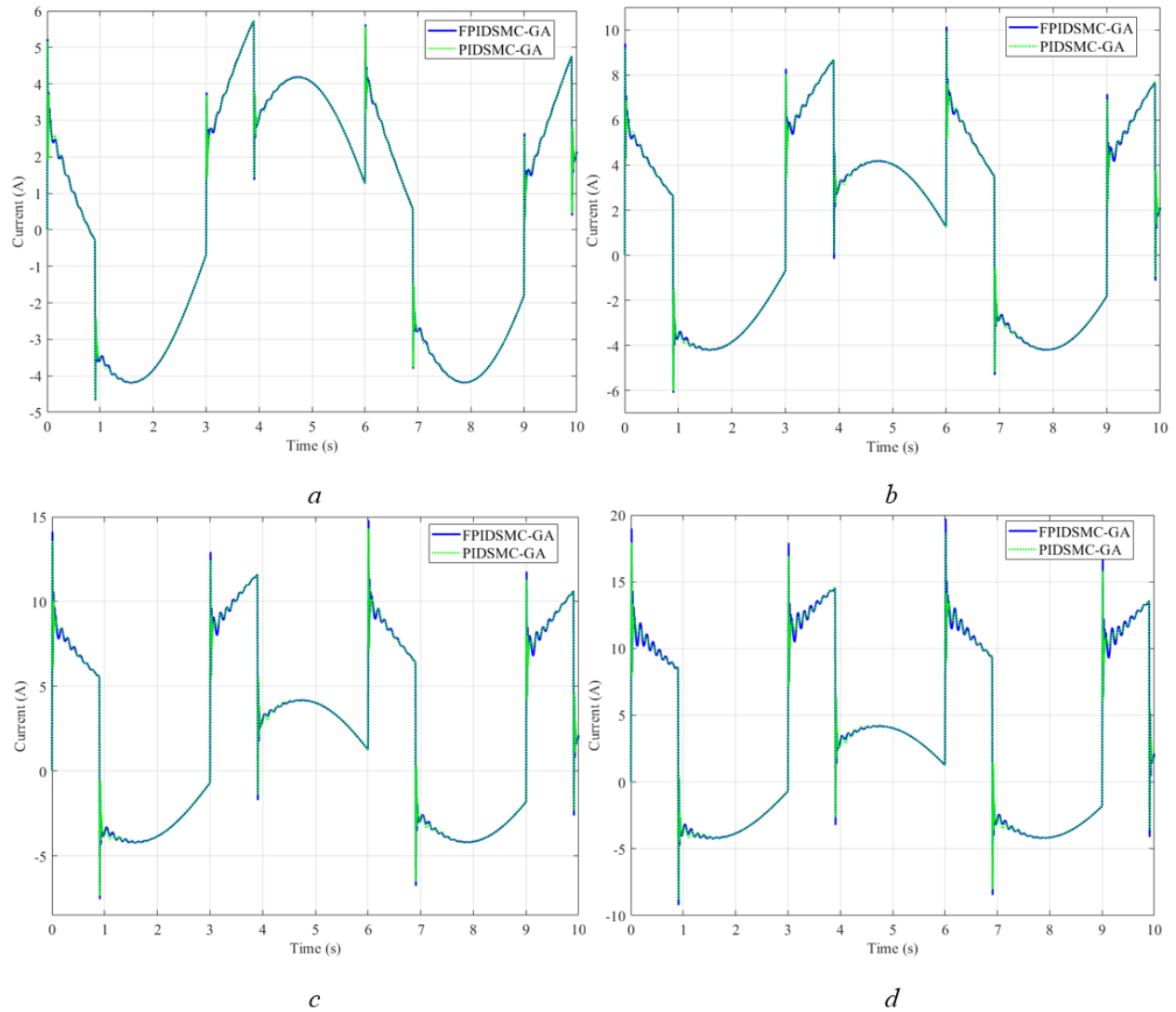


Figure 19. Current – The third case

(a)  $T_r = 2$  Nm, (b)  $T_r = 4$  Nm, (c)  $T_r = 6$  Nm, (d)  $T_r = 8$  Nm

In the first condition ( $A = 1$  rad,  $\omega = 1$  rad/s), the output signals follow the reference signal if the excitation from the road surface is small. If the value of  $T_r$  increases, the error also increases proportionally. In the third case, the output signal obtained from the PIDSMC-GA controller cannot follow the reference signal at many times. This can negatively affect system stability. However, if we use the fuzzy algorithm to adjust the parameters of the PIDSMC-GA controller (which becomes FPIDSMC-GA), the system's responsiveness and adaptation can be guaranteed.

In the second condition, the reference signal will be changed to investigate the adaptation of the new algorithm proposed in this research.

Table 7. Simulation results (3<sup>rd</sup> case – 1<sup>st</sup> condition)

	FPIDSMC-GA				PIDSMC-GA			
$T_r$ (Nm)	2	4	6	8	2	4	6	8
Error $\psi_{m\_max}$ (°)	0.97	1.63	2.26	3.32	2.53	4.78	7.05	9.41
Error $\psi_{m\_RMS}$ (°)	0.28	0.47	0.65	0.83	0.75	1.52	2.40	3.25
Error $\psi_{c\_max}$ (°)	0.15	0.20	0.28	0.40	0.20	0.37	0.55	0.75
Error $\psi_{c\_RMS}$ (°)	0.03	0.04	0.06	0.09	0.06	0.11	0.18	0.25
Value $i_{m\_max}$ (A)	5.74	10.14	14.81	19.71	5.75	9.93	14.32	18.70
Value $i_{m\_RMS}$ (A)	3.10	3.77	4.77	5.92	3.11	3.78	4.77	5.91

### 3.2.2. The second condition ( $A = 2 \text{ rad}$ , $\omega = 2 \text{ rad/s}$ )

In the second condition, the amplitude as well as the frequency of the reference signal are doubled. We investigate the changes in output signals in three cases.

#### The first case:

The first case uses periodic sinusoidal road surface noise as shown in Figure 8. Like in the first condition, the value of the motor angle obtained from the two controllers closely follows the reference signal (Figure 20). For PIDSMC-GA controller, the difference between the error is more considerable. In the first scenario, the resulting error values are  $1.12^\circ$  (max) and  $0.64^\circ$  (average) (Figure 20a). As  $T_r$  increases, the error values increase slightly to  $1.27^\circ$  and  $0.70^\circ$  for the second scenario (Figure 20b),  $1.54^\circ$  and  $0.85^\circ$  for the third scenario (Figure 20c) and  $1.81^\circ$  and  $0.96^\circ$  for the final scenario (Figure 20d). In general, the difference between these error values is not significant. For FPIDSMC-GA controller, an error of  $0.91^\circ$  (max) and  $0.27^\circ$  (average) is observed. These values do not change even though  $T_r$  increases (see results in Table 8). Optimizing controller parameters using the GA can help to ensure system stability under certain conditions.

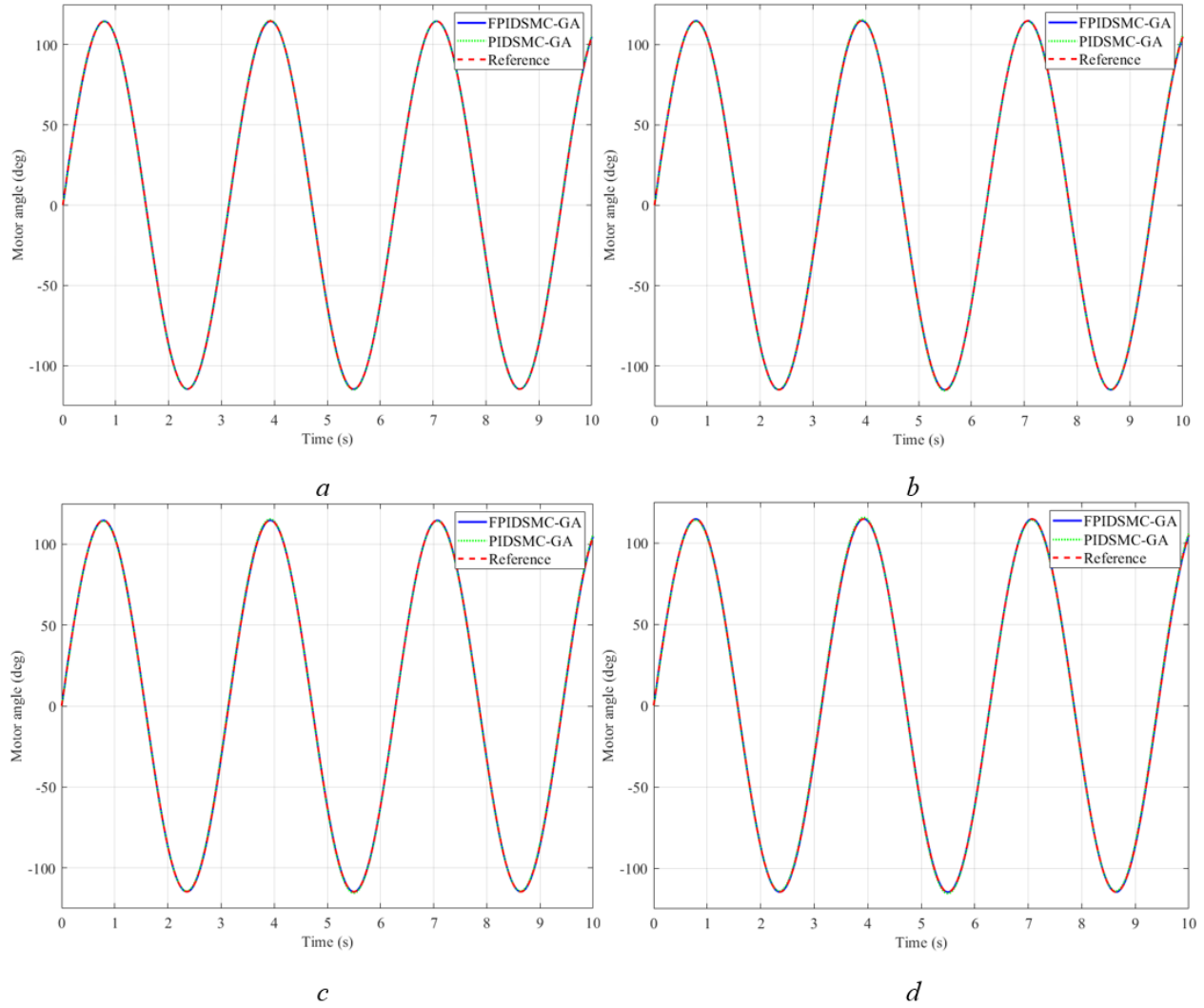


Figure 20. Motor angle – The first case

(a)  $T_r = 2$  Nm, (b)  $T_r = 4$  Nm, (c)  $T_r = 6$  Nm, (d)  $T_r = 8$  Nm

The difference in the values of steering column angle in these scenarios is not significant. According to Figure 21, the maximum difference between all scenarios is only  $0.42^\circ$  (for both simulation situations). Their average error value is only  $0.14^\circ$  for FPIDSMC-GA, which is  $0.01^\circ$  lower than the PIDSMC-GA scenario. This shows that optimizing the parameters of the integrated algorithm using the GA has the potential to increase system efficiency.

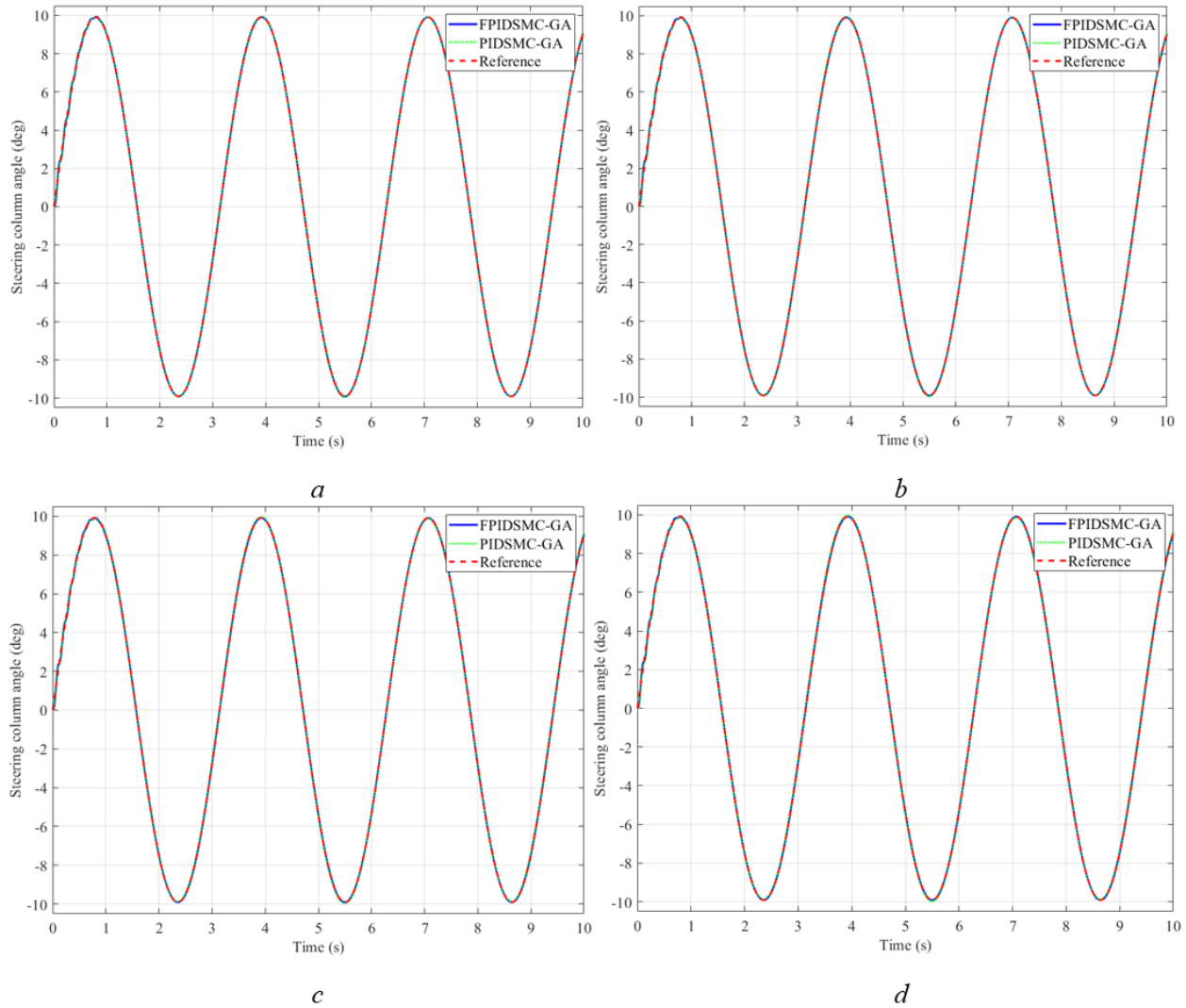


Figure 21. Steering column angle – The first case

(a)  $T_r = 2$  Nm, (b)  $T_r = 4$  Nm, (c)  $T_r = 6$  Nm, (d)  $T_r = 8$  Nm

In the second condition, the amplitude and frequency of the reference signal increase. In order for the output signal to accurately follow the set signal, the EPS system needs to use a larger current, i.e., consume more power than the first condition (Figure 13 and Figure 22). Figure 22a shows that the maximum value of  $i_m$  is 7.69A (PIDSMC-GA) and 7.75A (FPIDSMC-GA) when  $T_r = 2$ Nm. These figures increase sharply to 13.97A with  $T_r = 8$ Nm (Figure 22d). In conclusion, there is no difference in power consumption between the two scenarios: FPIDSMC-GA and PIDSMC-GA.

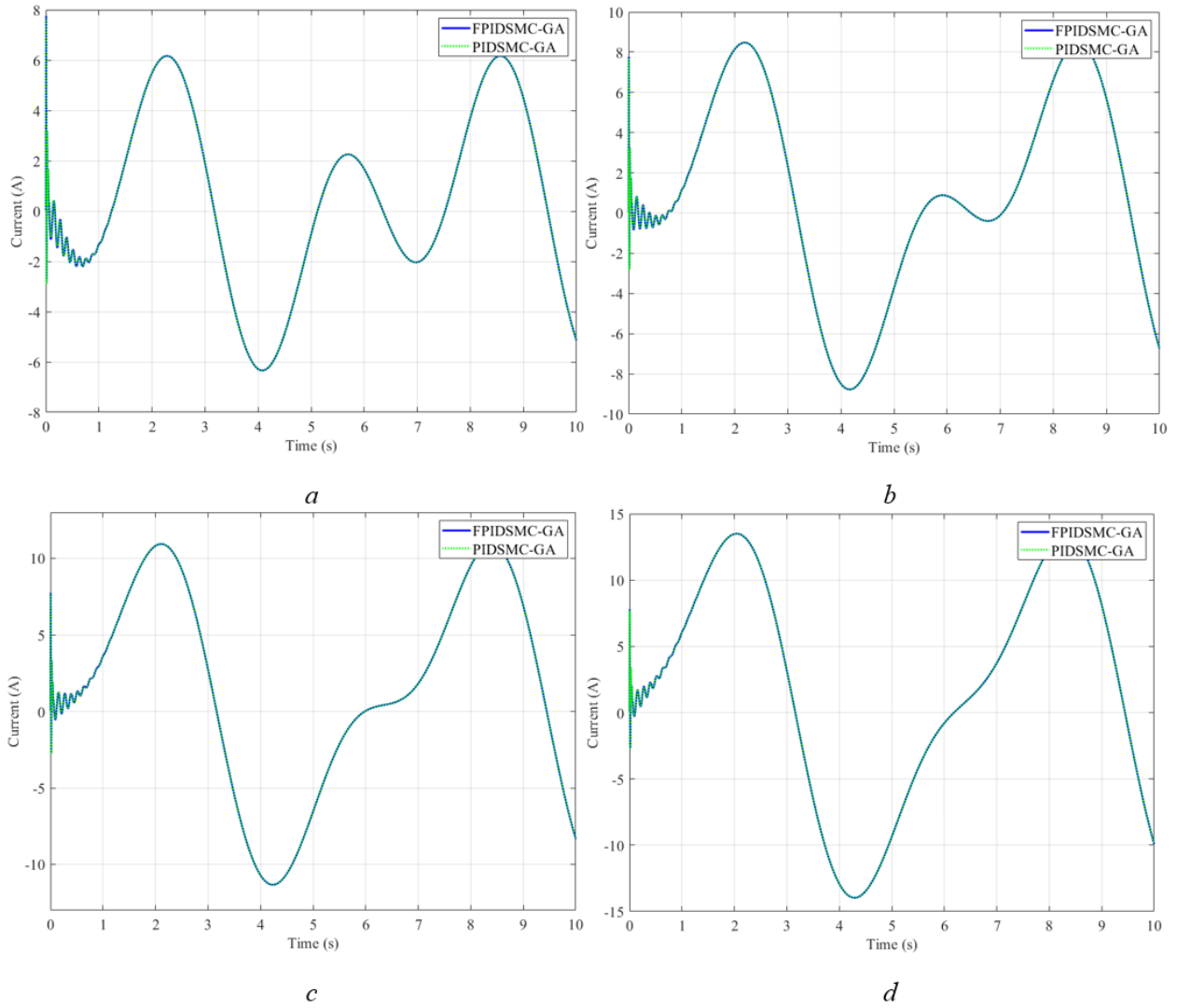


Figure 22. Current – The first case

(a)  $T_r = 2$  Nm, (b)  $T_r = 4$  Nm, (c)  $T_r = 6$  Nm, (d)  $T_r = 8$  Nm

Table 8. Simulation results (1<sup>st</sup> case – 2<sup>nd</sup> condition)

	FPIDSMC-GA				PIDSMC-GA			
	2	4	6	8	2	4	6	8
$T_r$ (Nm)	2	4	6	8	2	4	6	8
Error $\psi_{m\_max}$ (°)	0.91	0.91	0.91	0.91	1.12	1.27	1.54	1.81
Error $\psi_{m\_RMS}$ (°)	0.27	0.27	0.27	0.27	0.64	0.70	0.85	0.96
Error $\psi_{c\_max}$ (°)	0.42	0.42	0.42	0.42	0.42	0.42	0.42	0.42

<i>Error</i> $\psi_{c\_RMS}(\text{°})$	0.14	0.14	0.14	0.14	0.15	0.15	0.15	0.15
<i>Value</i> $i_{m\_max}(A)$	7.75	8.78	11.33	13.97	7.69	8.78	11.33	13.97
<i>Value</i> $i_{m\_RMS}(A)$	2.86	4.14	5.55	7.03	2.86	4.13	5.54	7.03

**The second case:**

The second case simulates the output signal variation under random disturbance from the road. As evident in Figure 23, the value of the motor angle obtained from both controllers closely follows the reference signal, with minor errors in the first and second scenarios. According to Table 9, the maximum error in the motor angle obtained from FPIDSMC-GA and the reference signal is only  $0.91^\circ$  for the first (Figure 23a), second (Figure 23b), and third (Figure 23c) scenarios. This value slightly increases to  $0.92^\circ$  (after rounding) for the final scenario (Figure 23d). The average values calculated according to RMS criteria are  $0.22^\circ$ ,  $0.25^\circ$ ,  $0.33^\circ$  and  $0.38^\circ$  for first, second, third and final scenarios respectively. These results demonstrate strong adaptability of the FPIDSMC-GA to the changes in simulation conditions.

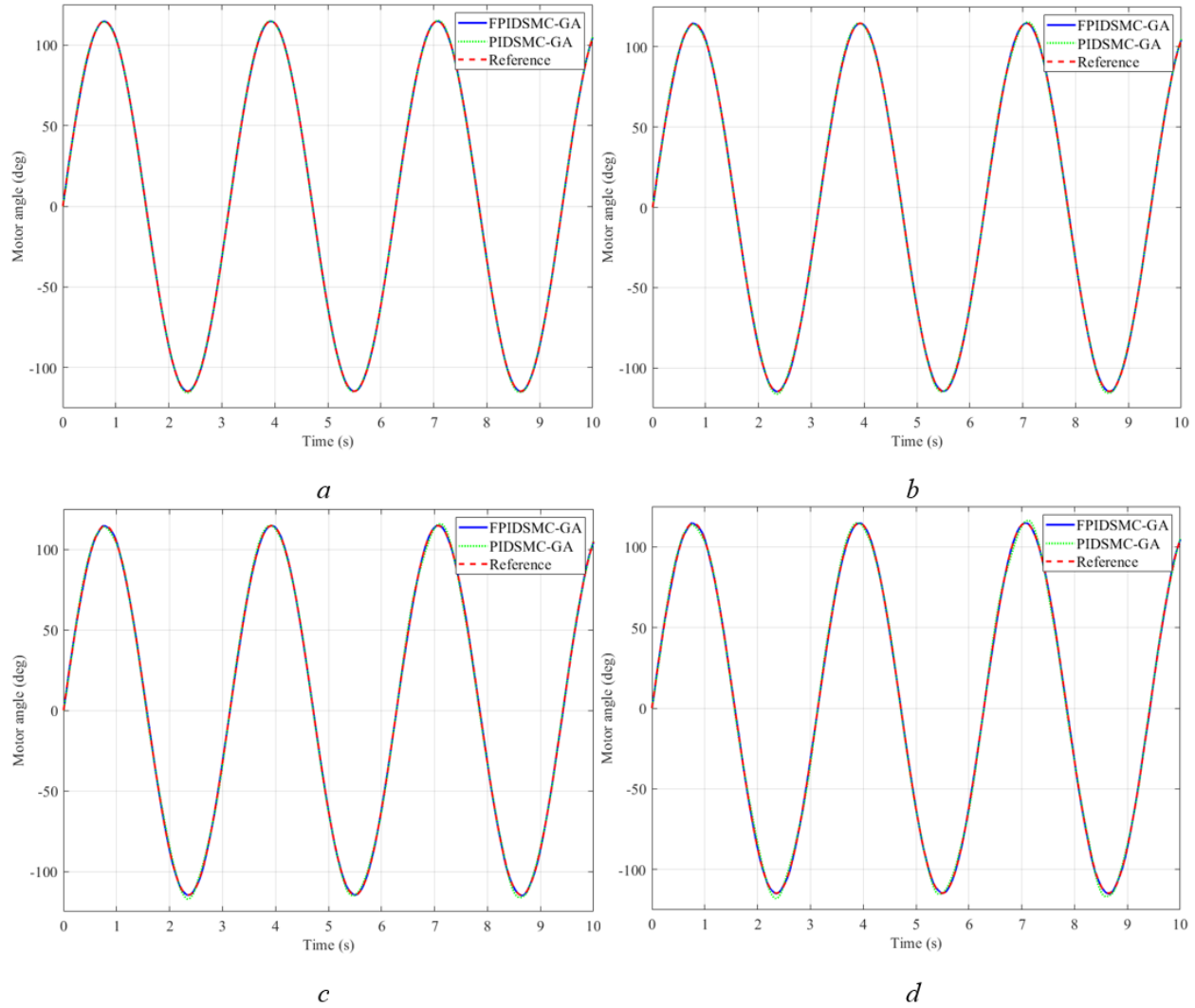


Figure 23. Motor angle – The second case

(a)  $T_r = 2$  Nm, (b)  $T_r = 4$  Nm, (c)  $T_r = 6$  Nm, (d)  $T_r = 8$  Nm

With the PIDSMC-GA, the system's stability is met only under certain conditions. In the first and second scenarios, the output follows the reference signals with an error not exceeding  $2^\circ$ . However, the error increases to nearly  $4^\circ$  in the final scenario (Figure 23d). The value of the steering column angle follows the desired signal in all the four scenarios when the PIDSMC-GA is used to control the EPS system (Figure 24). When the FPIDSMC-GA algorithm is applied to the system, the signal difference is similar to the one above. These results are presented in Table 9.

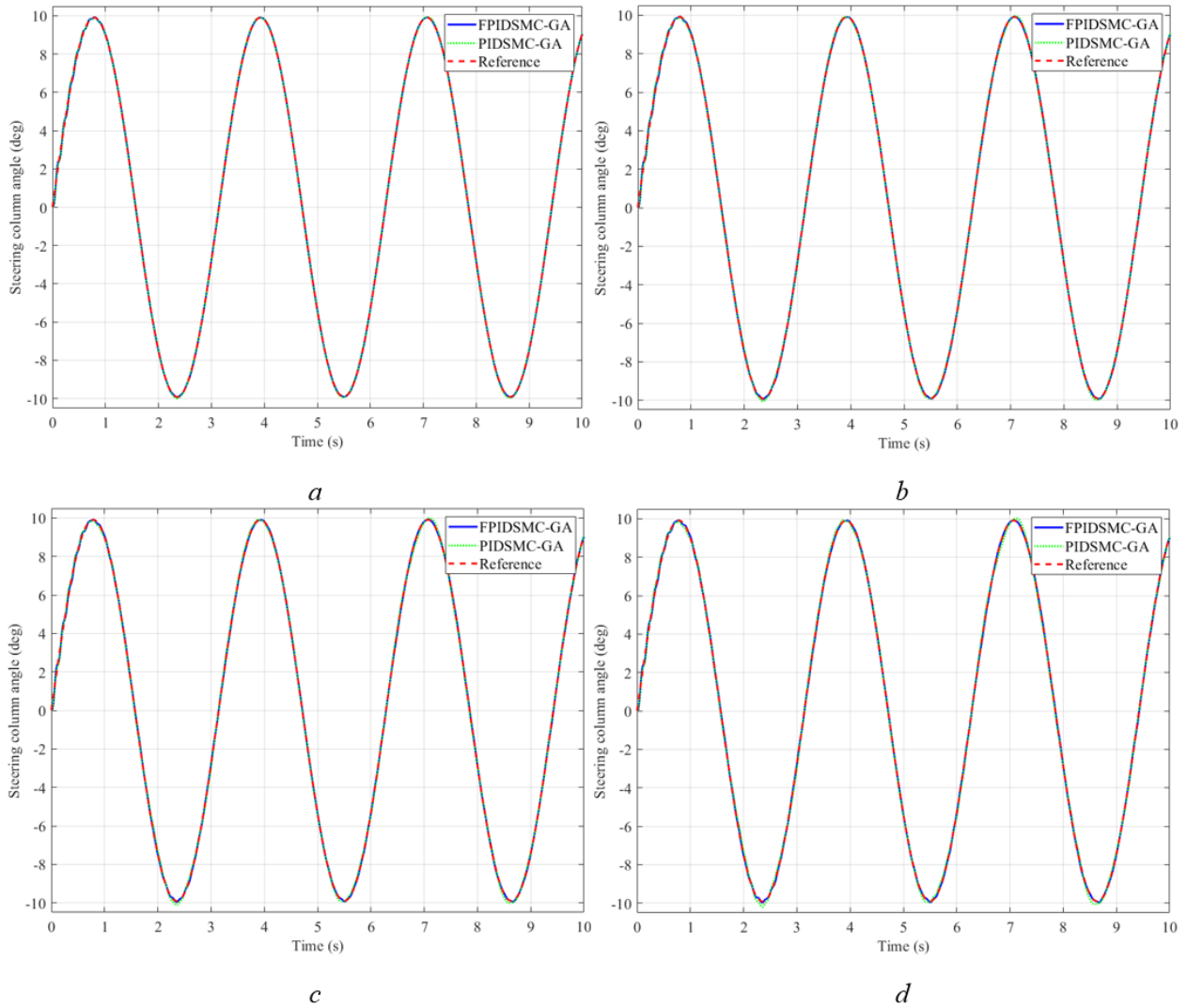


Figure 24. Steering column angle – The second case

(a)  $T_r = 2$  Nm, (b)  $T_r = 4$  Nm, (c)  $T_r = 6$  Nm, (d)  $T_r = 8$  Nm

Figure 25 illustrates energy consumption of the EPS system in the scenarios under discussion. Compared to the first condition, the current used in this condition has a more considerable value. As the road reaction torque increases, the peak as well as average values of current also increases.

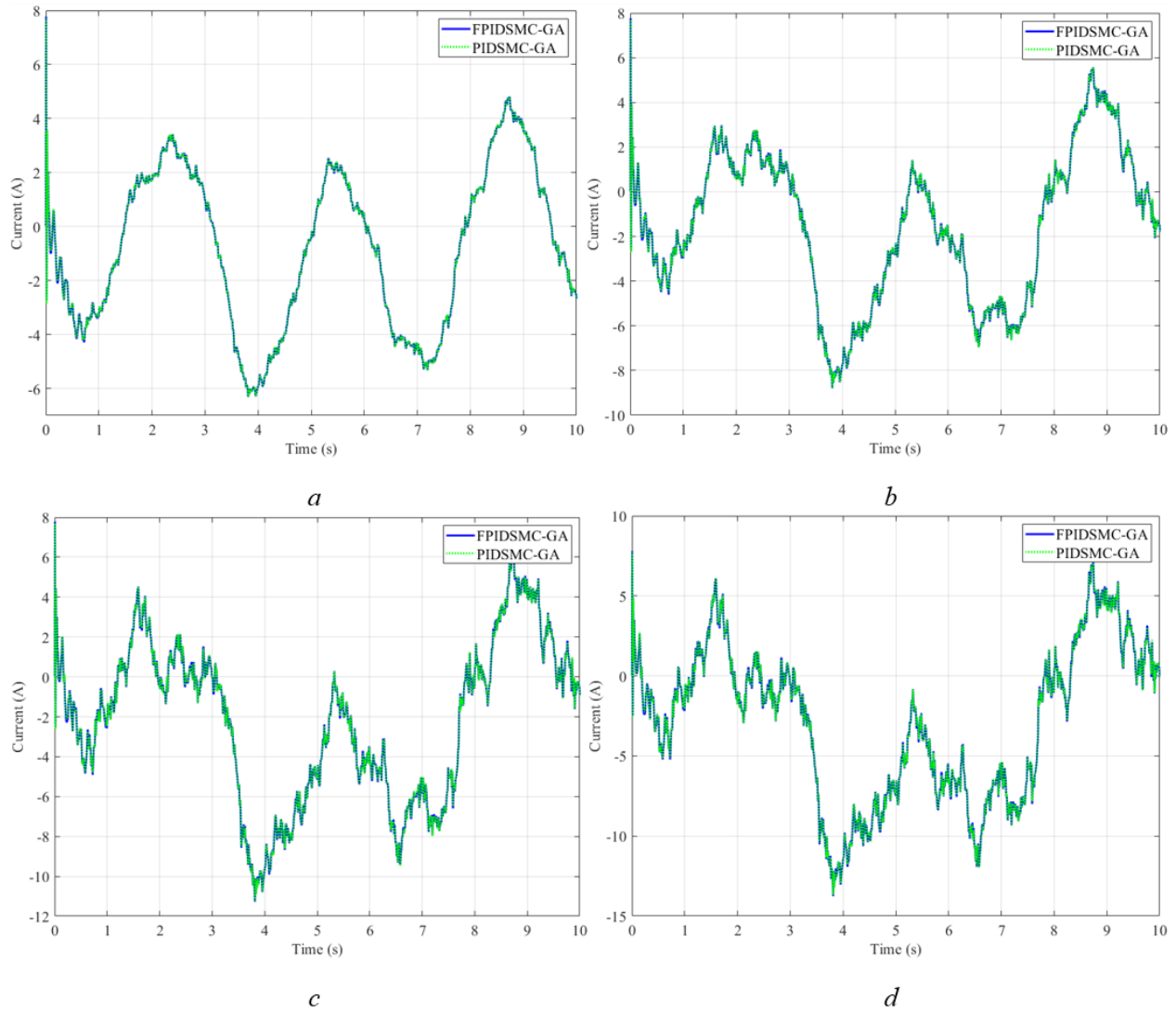


Figure 25. Current – The second case

(a)  $T_r = 2$  Nm, (b)  $T_r = 4$  Nm, (c)  $T_r = 6$  Nm, (d)  $T_r = 8$  Nm

Table 9. Simulation results (2<sup>nd</sup> case – 2<sup>nd</sup> condition)

	FPIDSMC-GA				PIDSMC-GA			
	$T_r$ (Nm)	2	4	6	8	2	4	6
$\psi_{m\_max}$ error (°)	0.91	0.91	0.91	0.92	1.73	1.98	2.78	3.86
$\psi_{m\_RMS}$ error (°)	0.22	0.25	0.33	0.38	0.74	0.95	1.30	1.61
$\psi_c\_max$ error (°)	0.42	0.42	0.42	0.42	0.42	0.42	0.42	0.42

$\psi_{c\_RMS}$ error (°)	0.09	0.05	0.09	0.09	0.11	0.08	0.13	0.15
$i_{m\_max}$ value (A)	7.77	8.79	11.27	13.74	7.71	8.75	11.21	13.67
$i_{m\_RMS}$ value (A)	2.77	3.31	3.91	4.70	2.77	3.32	3.91	4.71

**The third case:**

The difference between the signals is more evident in the third case. According to the research findings, the value of the motor angle obtained from the PIDSMC-GA controller cannot follow the desired signal (Figure 26). The error becomes higher at times corresponding to the excitation pulse from the road surface. The maximum difference between these two signals is found to be 2.48° for the first scenario (Figure 26a), 4.68° for the second scenario (Figure 26b), and 6.95° for the third scenario (Figure 26c). If road disturbance is increased up to 8 Nm, the difference between the actual and desired signals can be as high as 9.34° (Figure 26d). However, if we use the fuzzy algorithm to dynamically adjust the controller parameters, the error between the desired signal and the actual signal can be reduced. According to Table 10, the maximum error in the FPIDSMC-GA is only 5.73° for the fourth scenario (Figure 26d), while the average error in this case is only 0.63°, much smaller than the corresponding situation in the PIDSMC-GA based control law. In all the four scenarios, the output signal with the application of the FPIDSMC-GA follows the reference signal with negligible error.

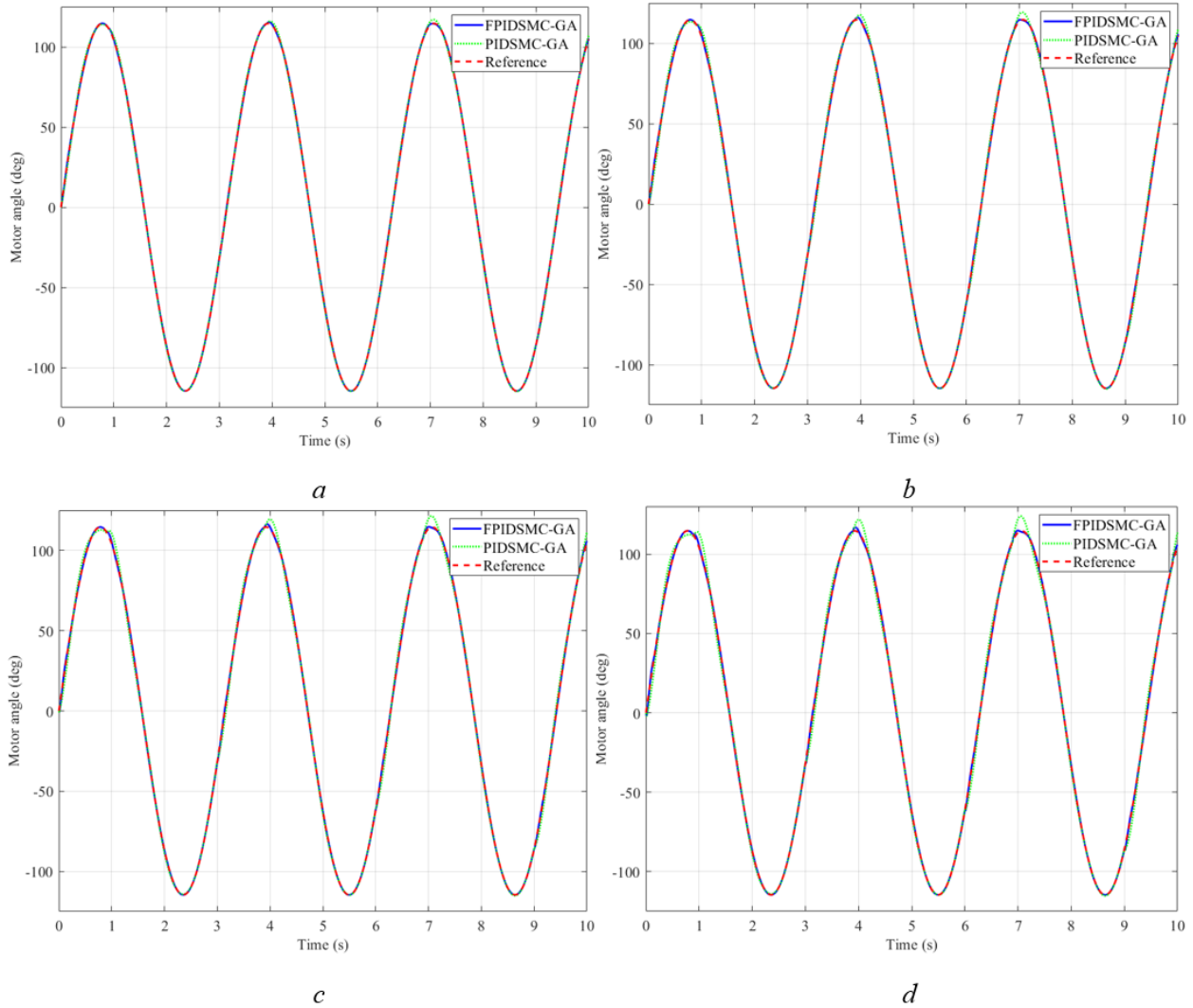


Figure 26. Motor angle – The third case

(a)  $T_r = 2$  Nm, (b)  $T_r = 4$  Nm, (c)  $T_r = 6$  Nm, (d)  $T_r = 8$  Nm

The results in Figure 27 show that the value of the steering column angle does not follow the desired signal when using the PIDSMC-GA controller. This phenomenon is observed in case of the second, third, and fourth scenarios (Figures 27b, 27c, and 27d). This can be improved by changing the parameters of the integrated controller based on the fuzzy principle. The FPIDSMC-GA intelligent hybrid algorithm helps in maintaining system stability under several complex conditions.

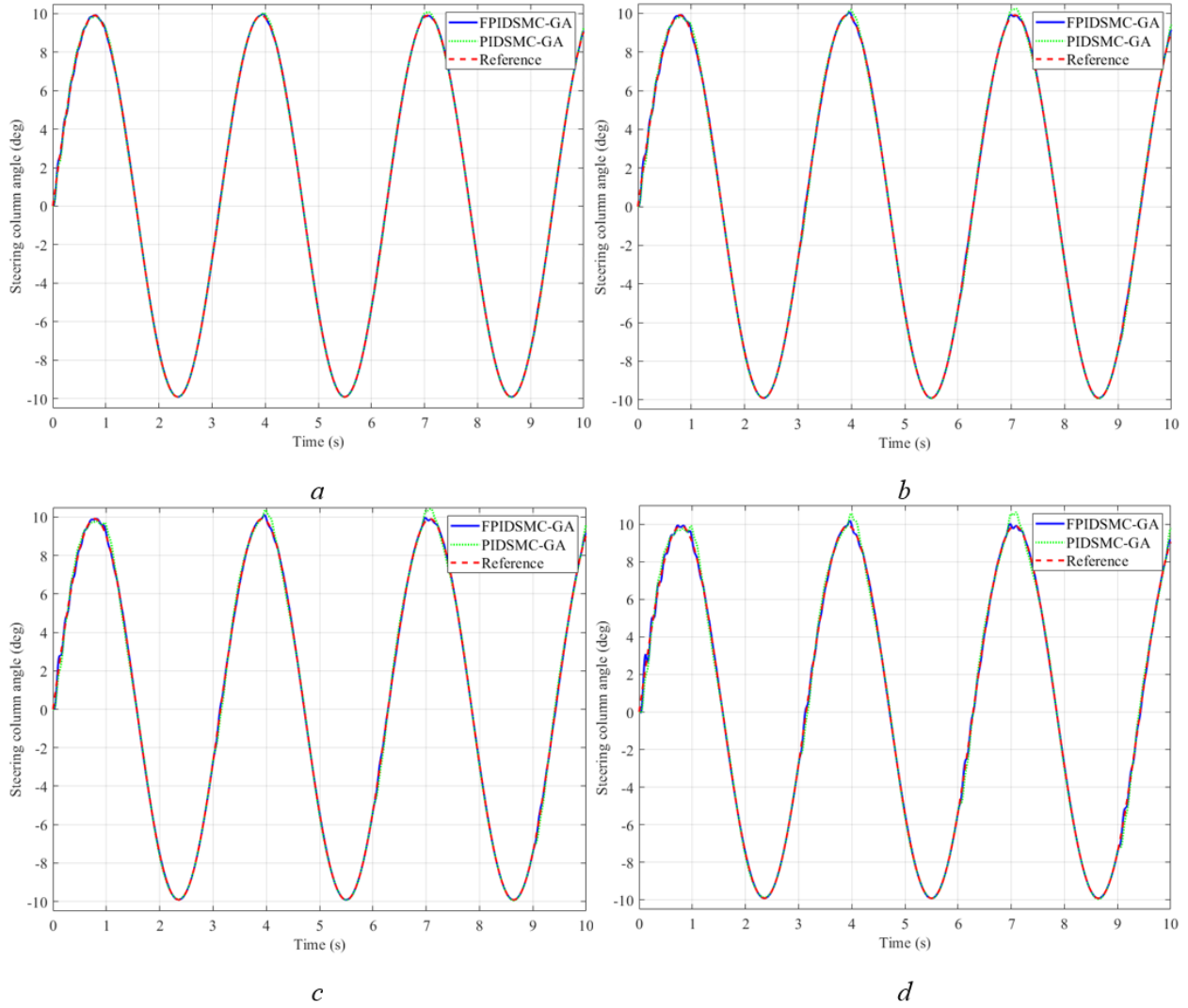


Figure 27. Steering column angle – The third case

(a)  $T_r = 2$  Nm, (b)  $T_r = 4$  Nm, (c)  $T_r = 6$  Nm, (d)  $T_r = 8$  Nm

In the last case, power consumption is the greatest. As illustrated in Figure 28, the value of current can be up to 20.61 A for the PIDSMC-GA situation and 21.72 A for the FPIDSMC-GA situation. Their corresponding RMS values are 4.34 A and 4.39 A respectively. Compared to the first condition, the peak value of the current increases but the RMS value decreases. In general, the current used in this case has a significant amplitude but is still within the allowable limit.

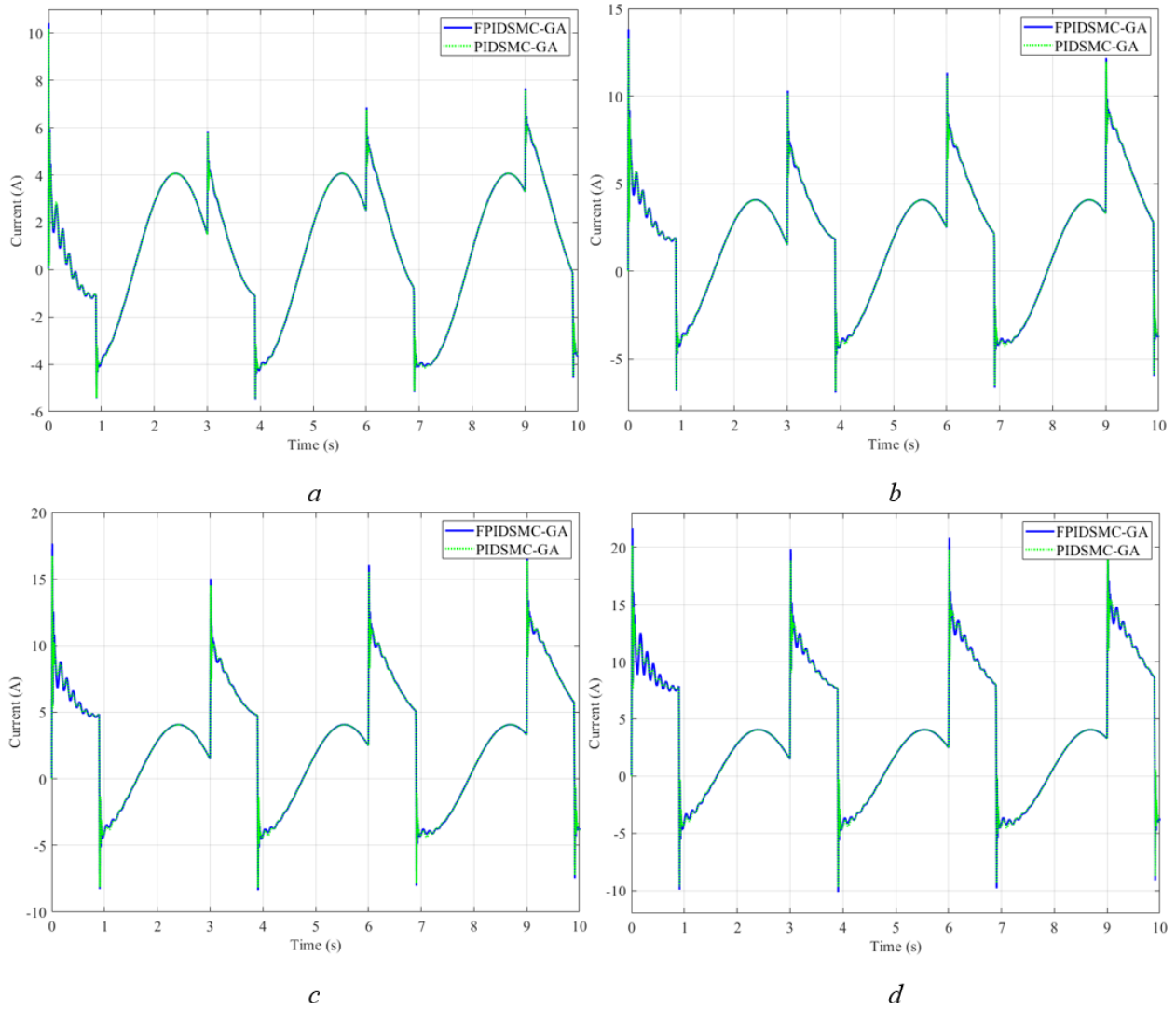


Figure 28. Current – The third case

(a)  $T_r = 2$  Nm, (b)  $T_r = 4$  Nm, (c)  $T_r = 6$  Nm, (d)  $T_r = 8$  Nm

Table 10. Simulation error results (3<sup>rd</sup> case – 2<sup>nd</sup> condition)

	FPIDSMC-GA				PIDSMC-GA				
	$T_r$ (Nm)	2	4	6	8	2	4	6	8
$\psi_{m\_max}$ error (°)		1.39	2.20	3.55	5.73	2.48	4.68	6.95	9.34
$\psi_{m\_RMS}$ error (°)		0.21	0.35	0.49	0.63	0.64	1.02	1.51	2.04
$\psi_{c\_max}$ error (°)		0.46	0.52	0.61	0.81	0.47	0.55	0.68	0.92

$\psi_{c\_RMS}$ error (°)	0.02	0.03	0.05	0.07	0.05	0.07	0.11	0.15
$i_{m\_max}$ value (A)	10.41	13.82	17.65	21.72	10.19	13.30	16.73	20.61
$i_{m\_RMS}$ value (A)	3.30	3.45	3.80	4.39	3.30	3.43	3.77	4.34

### 3.2.3. Considering the influence of noise

In a control system, noise cannot be completely eliminated. Noise can be generated from several sources, such as sensors, measurements, and electronic device noise. The two aforementioned conditions in subsections 3.2.1 and 3.2.2 analyzes the influence of disturbances without considering noise. In this section, the influence of noise in simulations and derivations is considered. Simulations are performed under the most robust conditions ( $A = 2$  N/m,  $\omega = 2$  rad/s, and  $T_r = 8$  N/m).

#### The first case:

The change of state variables (motor angle, steering column angle, and current) in the first case is depicted in Figure 29. Figure 29a shows the change in motor angle, while Figure 29b provides information about the steering column angle. The difference in results between Figure 29a and Figure 20d (motor angle without noise) is negligible. The maximum error is unchanged ( $0.42^\circ$ ), while the RMS error is slightly reduced. This is true for both algorithms: FPIDSMC-GA and PIDSMC-GA. Under the influence of noise, the steering column angle signal (Figure 29b) is sometimes slightly affected. As a result, the signal experiences slight vibrations instead of following a smooth curve. However, this influence is not significant. The integrated algorithm designed in this article guarantees output signal stability.

The current signal strongly suffers from chattering because it is not the object being controlled (Figure 29c). Compared to the result in Figure 22d (without noise), the value of the current in this condition is increased. Simulation results show that the peak value and RMS value of the current are 16.63A and 8.59A respectively. These values are 2.66A and 1.56A higher than the corresponding values in the case of not considering noise. These results are obtained when the system is controlled by the FPIDSMC-GA based control law. The results for the PIDSMC-GA scenario are similar to those for FPIDSMC-GA.

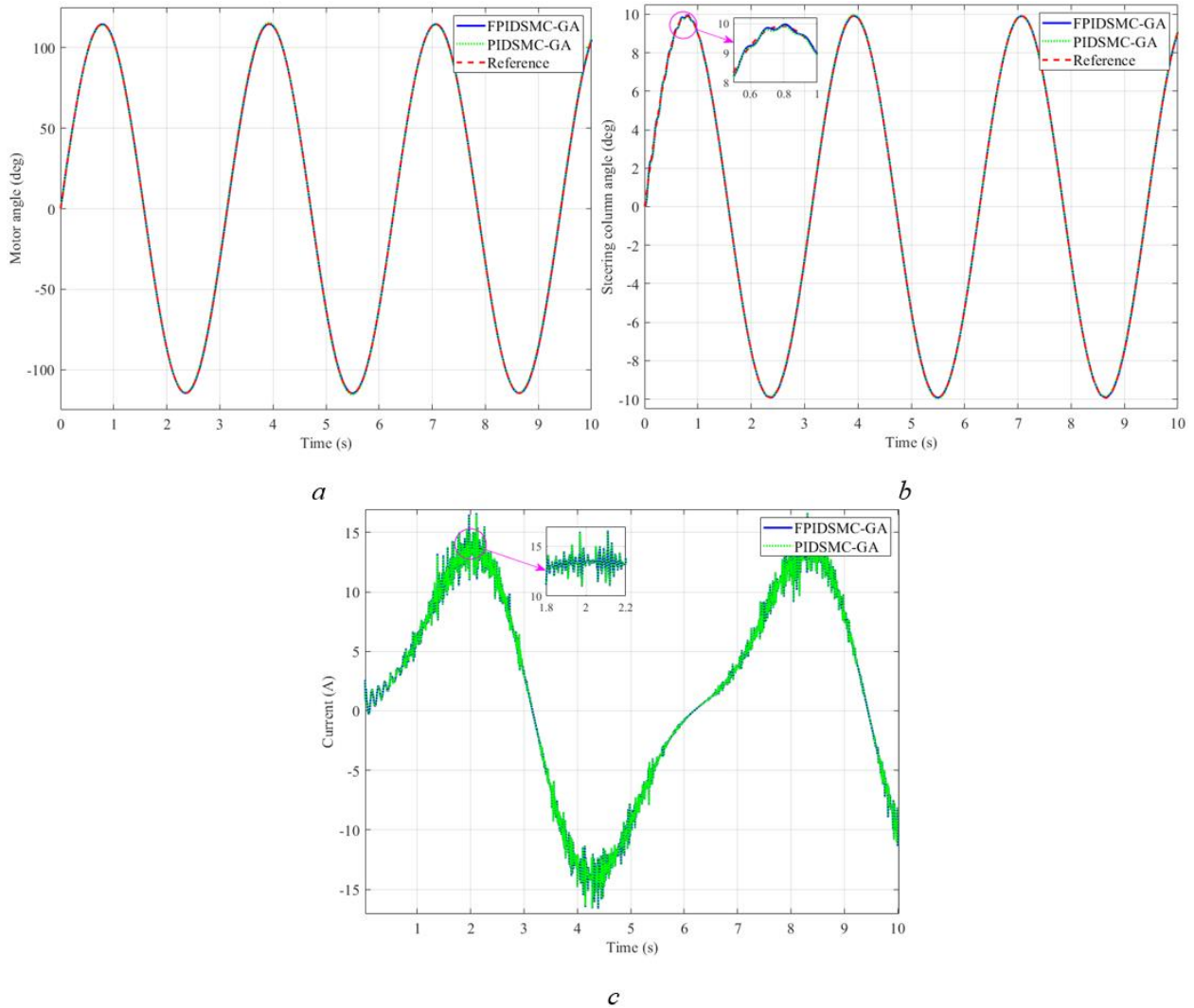


Figure 29. Simulation results with the noise – The first case

(a) Motor angle (b) Steering column angle (c) Current

### The second case:

Disturbances in the second case change continuously over time (the random function). The change in motor angle value is illustrated in Figure 30a. This is the controlled object, so its error is negligible even when the system is subjected to disturbances and noise. The maximum value of error in the motor angle is increased slightly by  $0.03^\circ$ . If the system is controlled by the PIDSMC-GA controller instead of the FPIDSMC-GA, the system error increases (see Table 11). Figure 30b shows that the steering column angle signal is affected by noise. However, this influence is not considerable and thus, it does not have a negative impact on the system.

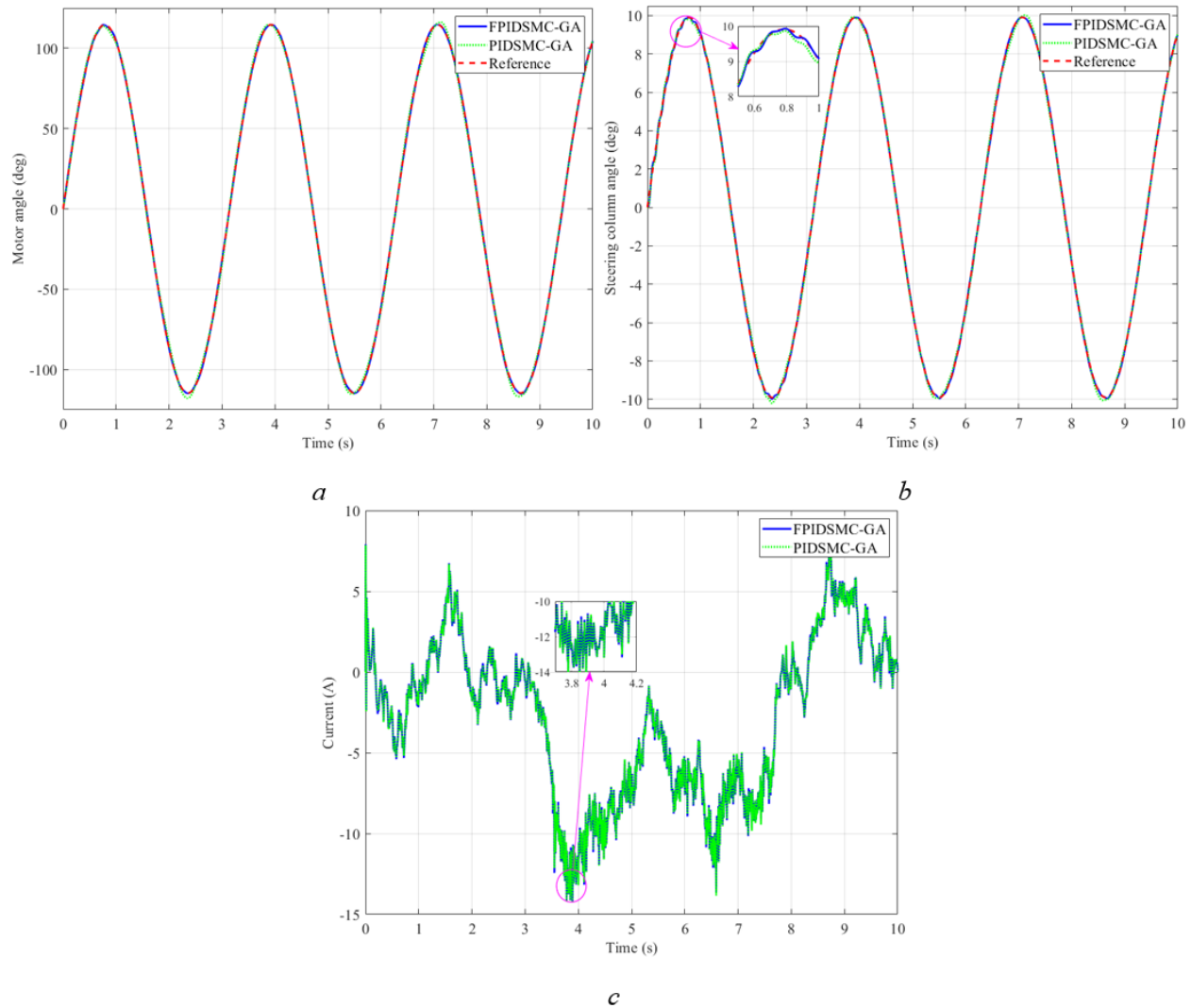


Figure 30. Simulation results with the noise – The second case

(a) Motor angle (b) Steering column angle (c) Current

According to Figure 30c, noise significantly affects the current signal. These values fluctuate continuously, causing the maximum error to increase from 13.74 to 14.17 and the RMS error from 4.70A to 5.35A when the system is controlled with the FPIDSMC-GA. The power consumption of the PIDSMC-GA controller is slightly larger than that of the FPIDSMC-GA.

### The third case:

Figure 31 illustrates the change in output values when subjected to disturbances (impulse signals) and system noise. Compared to the two cases mentioned above, the influence in this case is more evident. Depending on the level of disturbances and noise, the output signals experience chattering. The controlled object (motor angle) is only slightly chattered (Figure 31a), while the steering column angle (Figure 31b) and current signal (Figure 31c) are greatly affected. As a result, the system error is increased. Moreover, the power consumption in this case is also higher. Simulation results are listed in Table 11.

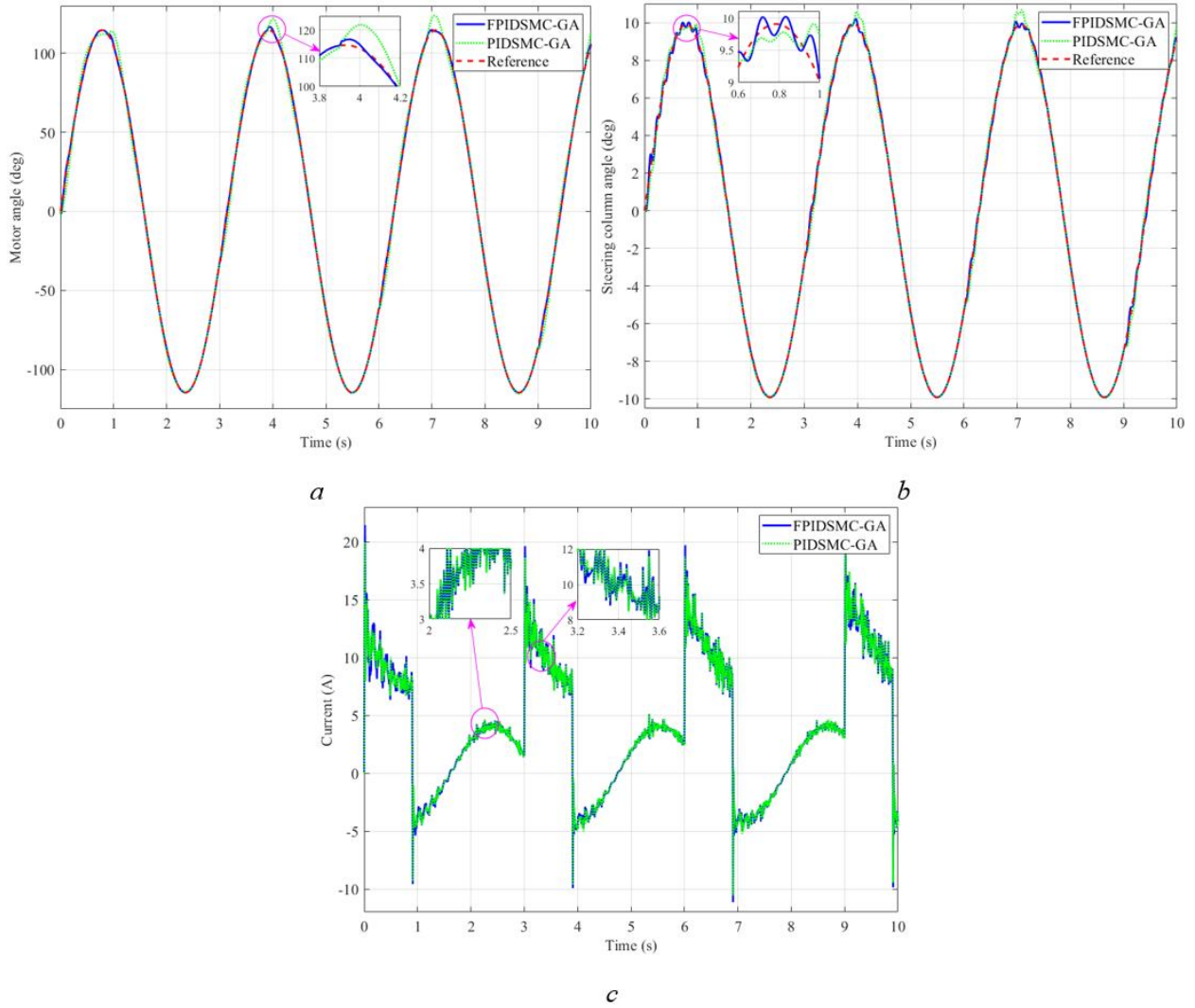


Figure 31. Simulation results with the noise – The third case

(a) Motor angle (b) Steering column angle (c) Current

Table 11. Simulation results (with noise).

	FPIDSMC-GA			PIDSMC-GA		
	Sine	Random	Pulse	Sine	Random	Pulse
$\psi_{m\_max}$ error (°)	0.89	0.95	5.38	1.83	3.93	9.40
$\psi_{m\_RMS}$ error (°)	0.14	0.32	0.57	0.96	1.70	3.32
$\psi_{c\_max}$ error (°)	0.42	0.42	0.78	0.42	0.42	0.89
$\psi_{c\_RMS}$ error (°)	0.05	0.06	0.10	0.08	0.14	0.26

$i_{m\_max}$ value (A)	16.63	14.17	21.50	16.59	14.21	20.31
$i_{m\_RMS}$ value (A)	8.59	5.35	5.05	8.59	5.36	5.03

Based on these results, we can make some remarks as follows:

- + Road disturbance significantly impacts the stability of the steering system. As the value of  $T_r$  increases, the error between the output signal and the desired signal also increases.
- + PIDSMC-GA optimally integrated controller can help to maintain system stability under certain conditions. However, system stability will not be guaranteed if road disturbances become more severe.
- + Flexibly changing the parameter values of the integrated controller is a suitable solution in the form of the FPIDSMC-GA. This change can help the system to adapt to external conditions. Therefore, it improves system stability under complex conditions.
- + Power consumption increases with the increase in road disturbance or the reference signal. When comparing the two scenarios, FPIDSMC-GA and PIDSMC-GA, we can see that the current used by them is the same.
- + For objects controlled by the FPIDSMC-GA, the influence of noise is not significant. Regarding other objects, chattering occurs when the system is subjected to disturbances and noise.

#### 4. Conclusion

In this research, we proposed the design of an optimally intelligent integrated algorithm FPIDSMC-GA to control the EPS system. A numerical simulation is performed to investigate the control performance. Road reaction torque  $T_r$  is considered as the external disturbance, and motor angle is the controlled signal. The value of  $T_r$  is varied in different scenarios. Simulation results demonstrate that the conventional optimization algorithm PIDSMC-GA cannot guarantee system stability under some complex conditions. To address this problem, we proposed FPIDSMC-GA which ensured that the values of the motor angle and steering column angle closely follow the set reference signal when the control law is used to control the EPS system. The error between the desired signal and the output signal is negligible, thus witnessing the superior performance of the FPIDSMC-GA based controller. The responsiveness and adaptability of the proposed control algorithm are guaranteed in several complex conditions. Therefore, the proposed control algorithm helps to improve system quality and stability.

While there are several salient features of the proposed hybrid control algorithm, the work also bears a few limitations mentioned here: 1) The current generated from the proposed controller is quite large, which increases the energy consumption; 2) The influence of external disturbances (road reaction torque) and system noise on the current is significant, which causes this signal to be chattered; 3) Membership functions are established based on previous simulation experience without optimization; 4) Road reaction torque is assumed to be known instead of being accurately

calculated using a vehicle dynamics model. 5) The optimal reference value range is selected empirically based on previous simulation calculations. In the future, we plan to add an optimally calculated object (current) according to the RMS criterion to solve the first limitation and to propose ideal optimization methods to replace the conventional fuzzy algorithm with an adaptive optimal fuzzy algorithm to solve problems 2 and 3. In addition, the fourth issue can be solved by using complex vehicle motion models. Finally, the fifth problem is planned to be solved using intelligent self-learning algorithms (such as ANFIS, reinforcement learning, or deep learning) to interpolate and predict the ideal value ranges of physical automotive EPS systems. Additionally, conducting future experiments on a physical testbed is planned to further demonstrate the performance of the proposed algorithm.

### **Declaration of conflicting interests**

The authors declare that there is no conflict of interest.

### **Reference**

- [1] Baek J, Kang C. Time-Delayed Control for Automated Steering Wheel Tracking of Electric Power Steering Systems. *IEEE Access* 2020; 8: 95457–64. <https://doi.org/10.1109/access.2020.2990970>.
- [2] Li S, Guo L, Cui G, Yu Z, Lu X, Wang G. Return Control of Electronic Power Steering Unequipped with an Angle Sensor. *International Journal of Automotive Technology* 2019; 20: 349–57. <https://doi.org/10.1007/s12239-019-0034-7>.
- [3] Choi JH, Nam K, Oh S. Steering feel improvement by mathematical modeling of the Electric Power Steering system. *Mechatronics* 2021; 78: 102629. <https://doi.org/10.1016/j.mechatronics.2021.102629>.
- [4] Anthonysamy B, et al. Subjective and Objective Steering Feel Evaluation of Compact SUV Electric Power Steering System Using Hardware in the Loop Simulation. *SAE Technical Paper Series* 2021. <https://doi.org/10.4271/2021-26-0080>.
- [5] Jie C, Yanling G. Research on Control Strategy of the Electric Power Steering System for All-Terrain Vehicles Based on Model Predictive Current Control. *Mathematical Problems in Engineering* 2021; 2021: 6642042. <https://doi.org/10.1155/2021/6642042>.
- [6] Chung S, Lee H. Advanced control strategy for electric power steering system to improve steering assist torque stability. 2015 15<sup>th</sup> International Conference on Control, Automation and Systems (ICCAS) 2015. <https://doi.org/10.1109/iccas.2015.7364696>.
- [7] Chung SS, Lee YZ, Kim ES. Development of the Wear Resistant Ball Nut Assembly in the Rack-Based Electric Power Steering. *International Journal of Automotive Technology* 2020; 21: 713–8. <https://doi.org/10.1007/s12239-020-0069-9>.
- [8] Kim K, Kim B, Go Y, Park J, Park J, Suh I, et al. An investigation on motor-driven power steering-based crosswind disturbance compensation for the reduction of driver steering effort. *Vehicle System Dynamics* 2014; 52: 922–47. <https://doi.org/10.1080/00423114.2014.909941>.

- [9] Jung D, Kim S. A Novel Control Strategy of Crosswind Disturbance Compensation for Rack-Type Motor Driven Power Steering (R-MDPS) System. *IEEE Access* 2022; 10: 125148–66. <https://doi.org/10.1109/access.2022.3225359>.
- [10] Marouf A, Djemai M, Sentouh C, Pudlo P. Driver torque and road reaction force estimation of an Electric Power Assisted Steering using sliding mode observer with unknown inputs. 13<sup>th</sup> International IEEE Conference on Intelligent Transportation Systems 2010. <https://doi.org/10.1109/itsc.2010.5625043>.
- [11] Jang B, Lee D, Kim K, Kim K-S. Road Torque Modeling for Electric Power Steering Systems. *International Journal of Automotive Technology* 2022; 23: 765–73. <https://doi.org/10.1007/s12239-022-0068-0>.
- [12] Ullah M I, Ajwad S A, Irfan M and Iqbal J. Non-linear control law for articulated serial manipulators: Simulation augmented with hardware implementation. *Elektronika Ir Elektrotehnika* 2016; 22: 3-7. <https://doi.org/10.5755/j01.eee.22.1.14094>
- [13] Hassan MK, Azubir NAM, Nizam HMI, Toha SF, Ibrahim BSKK. Optimal Design of Electric Power Assisted Steering System (EPAS) Using GA-PID Method. *Procedia Engineering* 2012; 41: 614–21. <https://doi.org/10.1016/j.proeng.2012.07.220>.
- [14] Baizid K, Yousnadj A, Meddahi A, Chellali R, Iqbal J. Time scheduling and optimization of industrial robotized tasks based on genetic algorithms. *Robotics and Computer-Integrated Manufacturing* 2015; 34: 140–50. <https://doi.org/10.1016/j.rcim.2014.12.003>.
- [15] Abu Hanifah R, Toha SF, Hassan MK, Ahmad S. Power reduction optimization with swarm based technique in electric power assist steering system. *Energy* 2016; 102: 444–52. <https://doi.org/10.1016/j.energy.2016.02.050>.
- [16] Hanifah RA, Toha SF, Ahmad S, Hassan MohdK. Swarm-Intelligence Tuned Current Reduction for Power-Assisted Steering Control in Electric Vehicles. *IEEE Transactions on Industrial Electronics* 2018; 65: 7202–10. <https://doi.org/10.1109/tie.2017.2784344>.
- [17] Zheng Z, Wei J. Research on electric power steering fuzzy PI control strategy based on phase compensation. *International Journal of Dynamics and Control* 2022; 11: 1867–79. <https://doi.org/10.1007/s40435-022-01077-2>.
- [18] Hassan MK, Aziah N, Nizam HMI, Mutalib AGA, Toha SF, Ibrahim BSKK. A comparative study of power consumption of electric power steering system. 2012 IEEE International Conference on Power and Energy (PECon) 2012. <https://doi.org/10.1109/pecon.2012.6450201>.
- [19] Li Y, Wu G, Wu L, Chen S. Electric power steering nonlinear problem based on proportional–integral–derivative parameter self-tuning of back propagation neural network. *Proceedings of the Institution of Mechanical Engineers, Part C: Journal of Mechanical Engineering Science* 2020;234:4725–36. <https://doi.org/10.1177/0954406220926549>.
- [20] Nguyen DN, Nguyen TA. Evaluate the stability of the vehicle when using the active suspension system with a hydraulic actuator controlled by the OSMC algorithm. *Scientific Reports* 2022; 12. <https://doi.org/10.1038/s41598-022-24069-w>.
- [21] Chitu C, Lackner J, Horn M, Srikanth Pullagura P, Waser H, Kohlböck M. Controller design for an electric power steering system based on LQR techniques. *COMPEL - The*

- International Journal for Computation and Mathematics in Electrical and Electronic Engineering 2013; 32: 763–75. <https://doi.org/10.1108/03321641311305737>.
- [22] Irmer M, Henrichfreise H. Design of a robust LQG Compensator for an Electric Power Steering. IFAC-PapersOnLine 2020; 53: 6624–30. <https://doi.org/10.1016/j.ifacol.2020.12.082>.
- [23] Yamamoto K, Sename O, Koenig D, Moulaire P. Design and experimentation of an LPV extended state feedback control on Electric Power Steering systems. Control Engineering Practice 2019; 90: 123–32. <https://doi.org/10.1016/j.conengprac.2019.06.004>.
- [24] Na S, Li Z, Qiu F, Zhang C. Torque Control of Electric Power Steering Systems Based on Improved Active Disturbance Rejection Control. Mathematical Problems in Engineering 2020; 2020: 6509607. <https://doi.org/10.1155/2020/6509607>.
- [25] Marouf A, Djemai M, Sentouh C, Pudlo P. A New Control Strategy of an Electric-Power-Assisted Steering System. IEEE Transactions on Vehicular Technology 2012; 61: 3574–89. <https://doi.org/10.1109/tvt.2012.2209689>.
- [26] Lee D, Jang B, Han M, Kim K-S. A new controller design method for an electric power steering system based on a target steering torque feedback controller. Control Engineering Practice 2021; 106: 104658. <https://doi.org/10.1016/j.conengprac.2020.104658>.
- [27] Lee D, Kim K-S, Kim S. Controller Design of an Electric Power Steering System. IEEE Transactions on Control Systems Technology 2018; 26: 748–55. <https://doi.org/10.1109/tcst.2017.2679062>.
- [28] Ma X, Guo Y, Chen L. Active disturbance rejection control for electric power steering system with assist motor variable mode. Journal of the Franklin Institute 2018; 355: 1139–55. <https://doi.org/10.1016/j.jfranklin.2017.12.024>.
- [29] Lee D, Yi K, Chang S, Lee B, Jang B. Robust steering-assist torque control of electric-power-assisted-steering systems for target steering wheel torque tracking. Mechatronics 2018; 49: 157–67. <https://doi.org/10.1016/j.mechatronics.2017.12.007>.
- [30] Dannöhl C, Müller S, Ulbrich H.  $H_\infty$ -control of a rack-assisted electric power steering system. Vehicle System Dynamics 2012; 50: 527–44. <https://doi.org/10.1080/00423114.2011.603051>.
- [31] Zhao W, Li Y, Wang C, Zhao T, Gu X.  $H_\infty$  control of novel active steering integrated with electric power steering function. Journal of Central South University 2013; 20: 2151–7. <https://doi.org/10.1007/s11771-013-1719-0>.
- [32] Zhao W, Lin Y, Wei J, Shi G. Control strategy of a novel electric power steering system integrated with active front steering function. Science China Technological Sciences 2011; 54: 1515–20. <https://doi.org/10.1007/s11431-011-4393-1>.
- [33] Ahmad S, Uppal AA, Azam MR, Iqbal J. Chattering Free Sliding Mode Control and State Dependent Kalman Filter Design for Underground Gasification Energy Conversion Process. Electronics 2023; 12: 876. <https://doi.org/10.3390/electronics12040876>.
- [34] Anjum MB, Khan Q, Ullah S, Hafeez G, Fida A, Iqbal J, et al. Maximum Power Extraction from a Standalone Photo Voltaic System via Neuro-Adaptive Arbitrary Order Sliding Mode Control Strategy with High Gain Differentiation. Applied Sciences 2022; 12: 2773. <https://doi.org/10.3390/app12062773>.

- [35] Khan M F, Islam R U, and Iqbal J. Control strategies for robotic manipulators. IEEE International Conference on Robotics and Artificial Intelligence (ICRAI), Rawalpindi, Pakistan 2012: 26-33. <https://doi.org/10.1109/ICRAI.2012.6413422>
- [36] Nguyen TA. A New Approach to Selecting Optimal Parameters for the Sliding Mode Algorithm on an Automotive Suspension System. Complexity 2023; 2023: 9964547. <https://doi.org/10.1155/2023/9964547>.
- [37] Kim G, You S, Lee S, Shin D, Kim W. Robust Nonlinear Torque Control Using Steering Wheel Torque Model for Electric Power Steering System. IEEE Transactions on Vehicular Technology 2023; 72: 9555–60. <https://doi.org/10.1109/tvt.2023.3248301>.
- [38] Kim S, Choi M, Sung J. Experimental Verifications of Electric Power Steering Controller Based on Discrete-Time Sliding Mode Control with Disturbance Observer. International Journal of Automotive Technology 2023; 24: 883–8. <https://doi.org/10.1007/s12239-023-0072-z>.
- [39] Mehmood Y, Aslam J, Ullah N, Alsheikhy AA, Din EU, Iqbal J. Robust fuzzy sliding mode controller for a skid-steered vehicle subjected to friction variations. PLoS ONE 2021; 16: e0258909. <https://doi.org/10.1371/journal.pone.0258909>.
- [40] Nguyen TA. Design a new control algorithm AFSP (Adaptive Fuzzy – Sliding Mode – Proportional – Integral) for automotive suspension system. Advances in Mechanical Engineering 2023; 15: 168781322311541. <https://doi.org/10.1177/16878132231154189>.
- [41] Afifa R, Ali S, Pervaiz M, Iqbal J. Adaptive Backstepping Integral Sliding Mode Control of a MIMO Separately Excited DC Motor. Robotics 2023; 12: 105. <https://doi.org/10.3390/robotics12040105>.
- [42] Lin F-J, Hung Y-C, Ruan K-C. An Intelligent Second-Order Sliding-Mode Control for an Electric Power Steering System Using a Wavelet Fuzzy Neural Network. IEEE Transactions on Fuzzy Systems 2014; 22: 1598–611. <https://doi.org/10.1109/tfuzz.2014.2300168>.
- [43] Milla F, Duarte-Mermoud MA, Aguila-Camacho N. Hierarchical MPC Secondary Control for Electric Power System. Mathematical Problems in Engineering 2014; 2014: 397567. <https://doi.org/10.1155/2014/397567>.
- [44] Murilo A, Rodrigues R, Teixeira ELS, Santos MMD. Design of a Parameterized Model Predictive Control for Electric Power Assisted Steering. Control Engineering Practice 2019; 90: 331–41. <https://doi.org/10.1016/j.conengprac.2019.07.010>.
- [45] Zheng Z, Wei J. Research on active disturbance rejection control strategy of electric power steering system under extreme working conditions. Measurement and Control 2023. <https://doi.org/10.1177/00202940231192986>.
- [46] Jeong YW, Chung CC, Kim W. Nonlinear Hybrid Impedance Control for Steering Control of Rack-Mounted Electric Power Steering in Autonomous Vehicles. IEEE Transactions on Intelligent Transportation Systems 2020; 21: 2956–65. <https://doi.org/10.1109/tits.2019.2921893>.
- [47] Zhao W, Zhao T, Li Y, Wang C, Zhang Z, Duan T. Integration optimization of novel electric power steering system based on quality engineering theory. Journal of Central South University 2013; 20: 1519–26. <https://doi.org/10.1007/s11771-013-1643-3>.

- [48] Zhao W, Wang C, Yu L, Chen T. Performance optimization of electric power steering based on multi-objective genetic algorithm. *Journal of Central South University* 2013; 20: 98–104. <https://doi.org/10.1007/s11771-013-1464-4>.
- [49] Liu X, Pang H, Shang Y, Wu W. Optimal Design of Fault-Tolerant Controller for an Electric Power Steering System with Sensor Failures Using Genetic Algorithm. *Shock and Vibration* 2018; 2018: 1801589. <https://doi.org/10.1155/2018/1801589>.
- [50] Saifia D, Chadli M, Karimi HR, Labiod S. Fuzzy control for Electric Power Steering System with assist motor current input constraints. *Journal of the Franklin Institute* 2015; 352: 562–76. <https://doi.org/10.1016/j.jfranklin.2014.05.007>.
- [51] Nguyen DN, Nguyen TA. Proposing an original control algorithm for the active suspension system to improve vehicle vibration: Adaptive fuzzy sliding mode proportional-integral-derivative tuned by the fuzzy (AFSPIDF). *Heliyon* 2023; 9: e14210. <https://doi.org/10.1016/j.heliyon.2023.e14210>.
- [52] Kim W, Kang C, Son Y-S, Chung C. Nonlinear Steering Wheel Angle Control Using Self-Aligning Torque with Torque and Angle Sensors for Electrical Power Steering of Lateral Control System in Autonomous Vehicles. *Sensors* 2018; 18: 4384. <https://doi.org/10.3390/s18124384>.
- [53] Nguyen DN, Nguyen TA. Proposing a BSPID Control Strategy Considering External Disturbances for Electric Power Steering (EPS) Systems. *IEEE Access* 2023; 11: 143230–49. <https://doi.org/10.1109/ACCESS.2023.3343914>
- [54] Nguyen TA, Iqbal J, Tran TTH, Hoang TB. Application of Hybrid Control Algorithm on the Vehicle Active Suspension System to Reduce Vibrations. *Advances in Mechanical Engineering* 2024; 16. <https://doi.org/10.1177/16878132241239816>